

TECHNICAL SPECIFICATION



Ultrasonics – Pulse-echo scanners – Low-echo sphere phantoms and method for performance testing of gray-scale medical ultrasound scanners applicable to a broad range of transducer types



THIS PUBLICATION IS COPYRIGHT PROTECTED

Copyright © 2015 IEC, Geneva, Switzerland

All rights reserved. Unless otherwise specified, no part of this publication may be reproduced or utilized in any form or by any means, electronic or mechanical, including photocopying and microfilm, without permission in writing from either IEC or IEC's member National Committee in the country of the requester. If you have any questions about IEC copyright or have an enquiry about obtaining additional rights to this publication, please contact the address below or your local IEC member National Committee for further information.

IEC Central Office
3, rue de Varembe
CH-1211 Geneva 20
Switzerland

Tel.: +41 22 919 02 11
Fax: +41 22 919 03 00
info@iec.ch
www.iec.ch

About the IEC

The International Electrotechnical Commission (IEC) is the leading global organization that prepares and publishes International Standards for all electrical, electronic and related technologies.

About IEC publications

The technical content of IEC publications is kept under constant review by the IEC. Please make sure that you have the latest edition, a corrigenda or an amendment might have been published.

IEC Catalogue - webstore.iec.ch/catalogue

The stand-alone application for consulting the entire bibliographical information on IEC International Standards, Technical Specifications, Technical Reports and other documents. Available for PC, Mac OS, Android Tablets and iPad.

IEC publications search - www.iec.ch/searchpub

The advanced search enables to find IEC publications by a variety of criteria (reference number, text, technical committee,...). It also gives information on projects, replaced and withdrawn publications.

IEC Just Published - webstore.iec.ch/justpublished

Stay up to date on all new IEC publications. Just Published details all new publications released. Available online and also once a month by email.

Electropedia - www.electropedia.org

The world's leading online dictionary of electronic and electrical terms containing more than 30 000 terms and definitions in English and French, with equivalent terms in 15 additional languages. Also known as the International Electrotechnical Vocabulary (IEV) online.

IEC Glossary - std.iec.ch/glossary

More than 60 000 electrotechnical terminology entries in English and French extracted from the Terms and Definitions clause of IEC publications issued since 2002. Some entries have been collected from earlier publications of IEC TC 37, 77, 86 and CISPR.

IEC Customer Service Centre - webstore.iec.ch/csc

If you wish to give us your feedback on this publication or need further assistance, please contact the Customer Service Centre: csc@iec.ch.

TECHNICAL SPECIFICATION



Ultrasonics – Pulse-echo scanners – Low-echo sphere phantoms and method for performance testing of gray-scale medical ultrasound scanners applicable to a broad range of transducer types

INTERNATIONAL
ELECTROTECHNICAL
COMMISSION

ICS 11.040.50; 17.140.50

ISBN 978-2-8322-2902-6

Warning! Make sure that you obtained this publication from an authorized distributor.

CONTENTS

FOREWORD.....	6
INTRODUCTION.....	8
1 Scope.....	10
2 Normative references	10
3 Terms and definitions	10
4 Symbols	12
5 General and environmental conditions	13
6 Equipment required	14
6.1 General.....	14
6.2 Phantom geometries	14
6.2.1 Phantoms for use in the frequency range 2 MHz to 7 MHz	14
6.2.2 Phantoms for use in the frequency range 7 MHz to 15 MHz including "micro-convex" arrays.....	14
6.2.3 Total internal-reflection surfaces.....	15
6.2.4 Spatially random distribution of low-echo spheres.....	15
6.3 Ultrasonic properties of the tissue-mimicking (TM) phantoms.....	15
7 Data acquisition assuming a spatially random distribution of low-echo spheres	16
7.1 Methodology	16
7.2 Storage of digitized image data.....	17
7.3 Digital image files available from the scanner itself	18
7.4 Image archiving systems.....	18
8 Automated data analysis for quantifying low-echo sphere detectability	18
8.1 General.....	18
8.2 Computation of mean pixel values (<i>MPVs</i>)	18
8.3 Determination of the $LSNR_m$ -value for a given depth interval.....	21
8.3.1 Preliminaries	21
8.3.2 Computation of the $LSNR_n$ -values and $LSNR_m$ -value in a given depth interval	21
8.3.3 Standard error corresponding to each $LSNR_n$ -value.....	21
Annex A (informative) Example of a phantom for performance testing in the 2 MHz to 7 MHz frequency range.....	22
Annex B (informative) Illustrations of the computation of $LSNR_m$ -values as a function of depth	24
Annex C (informative) Sufficient number of data images to assure reproducibility of results	29
C.1 General.....	29
C.2 Phantom with low-echo sphere diameter 3,2 mm, having 2 spheres per millilitre	29
C.3 Phantom with 2 mm-diameter, low-echo spheres and 8 spheres per millilitre	32
Annex D (informative) Example of a phantom for performance testing in the 7 MHz to 15 MHz frequency range.....	36
Annex E (informative) Determination of low-echo sphere positions to within $D/8$ in x , y and z Cartesian coordinates.....	39
E.1 Procedure	39
E.2 Argument for the choice of seven <i>MPV</i> nearest-neighbour sites for determining the centres of low-echo spheres	40

Annex F (informative) Test of total internal reflection produced by alumina and plate-glass, plane reflectors	41
Annex G (informative) Results of a test of reproducibility of $LSNR_m$ versus depth for a phantom with 4 mm-diameter low-echo spheres and 2 spheres per millilitre	48
Annex H (informative) Results for low-echo sphere-concentration dependence of $LSNR_m$ versus depth for phantoms with 4 mm-diameter spheres	50
Annex I (informative) Results for low-echo sphere-concentration dependence of $LSNR_m$ versus depth for phantoms with 3,2 mm-diameter spheres	53
Annex J (informative) Comparison of two different makes of scanner with similar transducers and console settings	57
Annex K (informative) Special considerations for 3-D probes	59
K.1 3-D probes operating in 2-D imaging mode	59
K.2 2-D arrays operating in 3-D imaging mode for determining $LSNR_m$ -values as a function of depth for reconstructed images	59
K.3 Mechanically driven 3-D probes operating in 3-D imaging mode	59
Bibliography	60
Figure 1 – Flow chart	17
Figure 2 – Schematic of an image plane	20
Figure A.1 – End view of the phantom applicable for 2 MHz to 7 MHz showing the spatially random distribution of 4-mm diameter low-echo spheres	22
Figure A.2 – Top view of phantom with 4 mm-diameter, low-echo spheres	23
Figure B.1 – Convex-array image of a prototype 4 mm-diameter low-echo sphere phantom for use in the 2 MHz to 7 MHz frequency range	24
Figure B.2 – Auxiliary figures relating to Figure B.1	25
Figure B.3 – Results corresponding to Figures B.1 and B.2, demonstrating reproducibility	25
Figure B.4 – Results corresponding to Figures B.1, B.2 and B.3	26
Figure B.5 – One of 80 parallel linear-array images of the phantom containing 4 mm-diameter, low-echo spheres, at 4 MHz with focus at 3 cm	26
Figure B.6 – Three successive images of the set of 80, separated by $D/4$ equal to 1 mm	27
Figure B.7 – Results for the 4 cm-wide, 3 cm-focus, linear array addressed in Figures B.5 and B.6	27
Figure B.8 – Results for the 4 cm-wide, 3 cm-focus, linear array addressed in Figures B.5, B.6 and B.7, using all 80 image frames corresponding to Figure B.7	28
Figure C.1 – One image obtained from a phantom containing 3,2 mm-diameter, low-echo spheres by using a 4 MHz linear array focused at 3 cm	29
Figure C.2 – Reproducibility result for two independent sets of 70 images with a mean number of low-echo sphere centres that is about 15 per 5 mm-depth interval	30
Figure C.3 – Results obtained by using both sets of 70 independent images corresponding to Figure C.2	30
Figure C.4 – Sector image (curved array) at 4,5 MHz with multiple foci at 4 cm, 8 cm and 12 cm depths; the low-echo spheres are 3,2 mm in diameter	31
Figure C.5 – Reproducibility results for a multiple-lateral-focus (4 cm, 8 cm and 12 cm) case corresponding to Figure C.4	31
Figure C.6 – Reproducibility results for the case corresponding to Figure C.5, except that there is a single focus at 10 cm depth	32
Figure C.7 – Reproducibility results for the case corresponding to Figure C.5, except that there is a single focus at 4 cm depth	32

Figure C.8 – Image of the phantom containing 2 mm-diameter, low-echo spheres, made with a curved array having 1,5 cm radius of curvature, with its focus at 3 cm 33

Figure C.9 – Reproducibility results corresponding to Figure C.8 33

Figure C.10 – Results using all 100 images in the image set that gave rise to Figure C.9..... 34

Figure C.11 – Image of the phantom containing 2 mm-diameter, low-echo spheres, made with a high-frequency (15 MHz) linear array, laterally focused at 4 cm..... 34

Figure C.12 – Reproducibility results corresponding to Figure C.11 35

Figure C.13 – Results using all 200 images in the image set that gave rise to Figure C.12..... 35

Figure D.1 – End- and top-view diagrams of the phantom containing 2 mm-diameter, low-echo spheres for use in the 7 MHz to 15 MHz frequency range..... 37

Figure D.2 – Image obtained by using the phantom containing 2 mm-diameter, low-echo spheres and a pediatric transducer with a radius of curvature of about 1,5 cm 38

Figure F.1 – Average of 10 images obtained by using a phased array..... 42

Figure F.2 – Plot of the data with blue data computed in the left rectangle in Figure F.1 and red data computed in the right rectangle 42

Figure F.3 – Plot of the data when the reflector is on the right side with blue computed in the left rectangle and red computed in the right rectangle 43

Figure F.4 – The percentage by which the mean pixel values resulting from reflections differ from the mean pixel values not involving reflections 44

Figure F.5 – Wide sector (153°), 1 cm-radius-of-curvature transducer with alumina reflector on the left..... 45

Figure F.6 – Plot of the data with blue computed in the left rectangle in Figure F.5 and red computed in the right rectangle 45

Figure F.7 – Plot of the data when the reflector is on the right side with blue computed in the left rectangle and red computed in the right rectangle 46

Figure F.8 – The percentage by which the mean pixel values resulting from reflections differ from the mean pixel values not involving reflections 46

Figure G.1 – Example image of the phantom with a 4,2 MHz curved array and two low-echo spheres per millilitre 48

Figure G.2 – Reproducibility results corresponding to the image set, one of which is shown in Figure G.1 49

Figure H.1 – Example of an image from the image set giving rise to the results in Figure H.2; the phantom contained an average of one 4 mm-diameter, low-echo sphere per millilitre 50

Figure H.2 – Results corresponding to an image set, one of which is shown in Figure H.1 51

Figure H.3 – Example of an image from the data set giving rise to the results in Figure H.4; the phantom contained an average of two 4 mm-diameter, low-echo spheres per millilitre 51

Figure H.4 – Results corresponding to an image set, one of which is shown in Figure H.3 52

Figure I.1 – Example of an image from the 4 ml⁻¹ data set producing the results shown in Figure I.2 53

Figure I.2 – Results for the phantom containing four 3,2 mm-diameter, low-echo spheres per millilitre..... 54

Figure I.3 – Example of an image from the 2 ml⁻¹ data set producing the results shown in Figure I.4 54

Figure I.4 – Results for the phantom containing two 3,2 mm-diameter, low-echo spheres per millilitre..... 55

Figure I.5 – Example of an image from the 1 ml^{-1} data set producing the results shown in Figure I.6	55
Figure I.6 – Results for the phantom containing one 3,2 mm-diameter, low-echo sphere per millilitre	56
Figure J.1 – Results for System A scanner and 7CF2 3-D (swept convex array) transducer focused at 4 cm and operated at 4,5 MHz in 2-D mode.....	57
Figure J.2 – Results for System B scanner with a 4DC7-3 3-D (convex array) transducer, operated at 4 MHz in 2-D mode and focused at 4 cm. The sector angle and all other console settings mimicked those for the System A case (Figure J.1)	57

INTERNATIONAL ELECTROTECHNICAL COMMISSION

ULTRASONICS – PULSE-ECHO SCANNERS – LOW-ECHO SPHERE PHANTOMS AND METHOD FOR PERFORMANCE TESTING OF GRAY-SCALE MEDICAL ULTRASOUND SCANNERS APPLICABLE TO A BROAD RANGE OF TRANSDUCER TYPES

FOREWORD

- 1) The International Electrotechnical Commission (IEC) is a worldwide organization for standardization comprising all national electrotechnical committees (IEC National Committees). The object of IEC is to promote international co-operation on all questions concerning standardization in the electrical and electronic fields. To this end and in addition to other activities, IEC publishes International Standards, Technical Specifications, Technical Reports, Publicly Available Specifications (PAS) and Guides (hereafter referred to as "IEC Publication(s)"). Their preparation is entrusted to technical committees; any IEC National Committee interested in the subject dealt with may participate in this preparatory work. International, governmental and non-governmental organizations liaising with the IEC also participate in this preparation. IEC collaborates closely with the International Organization for Standardization (ISO) in accordance with conditions determined by agreement between the two organizations.
- 2) The formal decisions or agreements of IEC on technical matters express, as nearly as possible, an international consensus of opinion on the relevant subjects since each technical committee has representation from all interested IEC National Committees.
- 3) IEC Publications have the form of recommendations for international use and are accepted by IEC National Committees in that sense. While all reasonable efforts are made to ensure that the technical content of IEC Publications is accurate, IEC cannot be held responsible for the way in which they are used or for any misinterpretation by any end user.
- 4) In order to promote international uniformity, IEC National Committees undertake to apply IEC Publications transparently to the maximum extent possible in their national and regional publications. Any divergence between any IEC Publication and the corresponding national or regional publication should be clearly indicated in the latter.
- 5) IEC itself does not provide any attestation of conformity. Independent certification bodies provide conformity assessment services and, in some areas, access to IEC marks of conformity. IEC is not responsible for any services carried out by independent certification bodies.
- 6) All users should ensure that they have the latest edition of this publication.
- 7) No liability should attach to IEC or its directors, employees, servants or agents including individual experts and members of its technical committees and IEC National Committees for any personal injury, property damage or other damage of any nature whatsoever, whether direct or indirect, or for costs (including legal fees) and expenses arising out of the publication, use of, or reliance upon, this IEC Publication or any other IEC Publications.
- 8) Attention is drawn to the Normative references cited in this publication. Use of the referenced publications is indispensable for the correct application of this publication.

The main task of IEC technical committees is to prepare International Standards. In exceptional circumstances, a technical committee may propose the publication of a Technical Specification when

- the required support cannot be obtained for the publication of an International Standard, despite repeated efforts, or
- the subject is still under technical development or where, for any other reason, there is the future but no immediate possibility of an agreement on an International Standard.

Technical Specifications are subject to review within three years of publication to decide whether they can be transformed into International Standards.

Technical Specification IEC TS 62791 has been prepared by IEC technical committee 87 Ultrasonics.

The text of this Technical Specification is based on the following documents:

DTS	Report on voting
87/554/DTS	87/570/RVC

Full information on the voting for the approval of this Technical Specification can be found in the report on voting indicated in the above table.

This publication has been drafted in accordance with the ISO/IEC Directives, Part 2.

Terms in **bold** in the text are defined in Clause 3.

The committee has decided that the contents of this publication will remain unchanged until the stability date indicated on the IEC website under "<http://webstore.iec.ch>" in the data related to the specific publication. At this date, the publication will be

- transformed into an International standard,
- reconfirmed,
- withdrawn,
- replaced by a revised edition, or
- amended.

IMPORTANT – The 'colour inside' logo on the cover page of this publication indicates that it contains colours which are considered to be useful for the correct understanding of its contents. Users should therefore print this document using a colour printer.

A bilingual version of this publication may be issued at a later date.

INTRODUCTION

Ultrasonic pulse-echo scanners are widely used in medical practice to produce images of soft tissue organs throughout the human body. Most ultrasonic pulse-echo scanners produce real-time images of tissue in a scan plane by sweeping a narrow, pulsed beam of ultrasound through the tissue section of interest and detecting the echoes generated by reflection at tissue boundaries and by scattering within tissues. Generally, the sweep that generates an image frame is repeated at least 20 times per second, giving rise to the real-time aspect of the displayed image. The axes of the pulsed beams generally lie in a plane that defines the scan plane.

Various transducer types are employed to operate in a transmit/receive mode to generate/detect the ultrasonic signals. Linear arrays, in which the beam axes are all parallel to one another, resulting in a rectangular image, consist of a line of hundreds of parallel transducer elements with a subset of adjacent elements producing one pulse at a time. Convex arrays are similar to linear arrays but the element arrangements define part of the surface of a short right circular cylinder with the array elements parallel to the axis of the cylinder. The radius of curvature of the cylinder (and therefore the array) can have values between 0,5 cm and 7 cm. The convex array generates a sector image since the beam axes fan out over the scan plane. A phased array has a linear arrangement of elements, where all elements act together to form a pulse and the direction and focus of an emitted pulse is determined by the timing of excitations of the elements. The phased array generates a sector image. Another type of sector scanner is the mechanical sector scanner in which a single element transducer or an annular array transducer is rotated about a fixed axis during pulse emissions. All the foregoing transducer types commonly operate within the frequency range 2 MHz to 15 MHz, to which this Technical Specification applies.

A 2-dimensional array (2-D array) is restricted to an array of transducer elements distributed over a square area or a spherical cap. Such an array receives echoes from a 3-D volume and can produce images corresponding to any planar surface in that volume. A 3-D mechanically driven, convex array (3-D MD convex array) means a convex array that acquires images as it is rotated mechanically about an axis lying in its image plane or an extension of that plane. A 3-D mechanically driven, linear array (3-D MD linear array) is similar to a 3-D MD convex array, where the array radius of curvature is infinite and the array is either rotated about an axis or is translated perpendicularly to the scan plane of the linear array. For an overview of current 3-D and 4-D systems, see sections 1.5 and 10.2.2 of [1]¹.

One means for testing the imaging performance of an ultrasound pulse-echo scanner is to quantify the degree to which a small cyst-like (low-echo) object is distinguished from the surrounding soft tissue, i.e. the degree to which a small cyst-like (low-echo) object is detectable in the surrounding soft tissue. It is reasonable to assume that the smaller the **low-echo sphere** that can be detected at some position, the better the resolution of the scanner, i.e. the better it will delineate the boundary of an abnormal object, such as a tumour. There are three components of resolution defined in pulse-echo ultrasound:

- axial resolution (parallel to the local pulse propagation direction);
- lateral resolution (perpendicular to the local pulse propagation direction and parallel to the scan plane); and
- elevational resolution (perpendicular to the local pulse propagation direction and also to the scan plane).

Axial resolution usually – but not always – is better than lateral and elevational resolutions. Thus, all three components should be given equal weight in measuring **detectability**. A sphere has no preferred orientation and is therefore the best shape for a cyst-like object for two reasons. First, all three components of resolution are weighted equally no matter what the beam's incident direction is. Second, the incident beam's propagation direction will vary

¹ The numbers in square brackets refer to the Bibliography.

considerably in the case of convex and phased arrays depending on where the object exists in the imaged volume.

It is important that the phantom allows quantification of **detectability** to be carried out over the entire depth range imaged; thus, it is important that the low-echo spheres exist up to the entire scanning window. A phantom limited to a flat scanning surface is acceptable for a linear array, phased array, or a flat 2-D array, but not for the remaining types of arrays. Each of the phantoms described in this Technical Specification contains a random distribution of equal diameter [2], low-echo spheres existing at all depths, including the case of those designed for testing convex (curved) arrays.

This Technical Specification summarizes the requirements for a phantom to provide for determination of **detectability** of low-echo (cyst-like) objects for any type of pulse-echo transducer, except (perhaps) a 2-D array with a spherical-cap surface.

The International Electrotechnical Commission (IEC) draws attention to the fact that it is claimed that compliance with this document may involve the use of US Patents 5,574,212 and 8,887,552, concerning an “Automated System and Method for Testing Resolution of Ultrasound Scanners” and an “Ultrasound Phantom Having a Curved Surface”, respectively, given in 8.2 and 8.3, and Annexes A and D.

IEC takes no position concerning the evidence, validity and scope of this patent right.

The holder of this patent right has assured the IEC that he/she is willing to negotiate licences under reasonable and non-discriminatory terms and conditions with applicants throughout the world. In this respect, the statement of the holder of this patent right is registered with IEC. Information may be obtained from:

Wisconsin Alumni Research Foundation,
614 Walnut Street, 13th Floor,
Madison, WI 53726,
USA

Attention is drawn to the possibility that some of the elements of this document may be the subject of patent rights other than those identified above. IEC shall not be held responsible for identifying any or all such patent rights.

ISO (www.iso.org/patents) and IEC (<http://patents.iec.ch>) maintain on-line data bases of patents relevant to their standards. Users are encouraged to consult the data bases for the most up to date information concerning patents.

ULTRASONICS – PULSE-ECHO SCANNERS – LOW-ECHO SPHERE PHANTOMS AND METHOD FOR PERFORMANCE TESTING OF GRAY-SCALE MEDICAL ULTRASOUND SCANNERS APPLICABLE TO A BROAD RANGE OF TRANSDUCER TYPES

1 Scope

This Technical Specification defines terms and specifies methods for quantifying the imaging performance of real-time, ultrasound B-mode scanners. The types of transducers used (see sections 7.6 and 10.7 of [1]) with these scanners include

- a) phased array,
- b) linear arrays,
- c) convex arrays,
- d) mechanical sector scanners,
- e) 3-D probes operating in 2-D imaging mode (see Annex K),
- f) 3-D probes operating in 3-D imaging mode for a limited number of sets of reconstructed 2-D images (see Annex K).

The test methodology is applicable for transducers operating in the 2 MHz to 15 MHz frequency range.

2 Normative references

The following documents, in whole or in part, are normatively referenced in this document and are indispensable for its application. For dated references, only the edition cited applies. For undated references, the latest edition of the referenced document (including any amendments) applies.

IEC 60050-802, *International Electrotechnical Vocabulary – Ultrasonics* (available at: <http://www.electropedia.org>)

IEC 61391-1, *Ultrasonics – Pulse-echo scanners – Part 1: Techniques for calibrating spatial measurement systems and measurement of system point-spread function response*

IEC 61391-2:2010, *Ultrasonics – Pulse-echo scanners – Part 2: Measurement of maximum depth of penetration and local dynamic range*

3 Terms and definitions

For the purposes of this document, the terms and definitions given in IEC 60050-802, IEC 61391-1 and the following apply.

3.1

active area of a transducer

area over which transducer transmitting and/or receiving elements are distributed

3.2

backscatter coefficient **intrinsic backscatter coefficient**

BSC

intrinsic property of a material at some frequency, equal to the differential scattering cross-section per unit volume for a scattering angle of 180°

Note 1 to entry: See [4], [5], [6].

[SOURCE: IEC 61391-1:2006, 3.6, modified]

3.3

low-echo sphere

spherical inclusion in a phantom with **backscatter coefficient** much lower than that of the background tissue-mimicking material

Note 1 to entry: All low-echo spheres in a phantom have the same diameter with a tolerance of $\pm 1\%$.

3.4

low-echo sphere diameter

D

diameter of the low-echo spherical inclusions in a phantom

Note 1 to entry: It is generally assumed that all **low-echo spheres** in a particular phantom have the same diameter *D*. The diameter tolerance is $\pm 1\%$.

3.5

pixel

smallest spatial unit or cell size of a digitized 2-dimensional array representation of an image

Note 1 to entry: Each **pixel** has an address corresponding to its position in the array.

Note 2 to entry: **Pixel** is a contraction of 'picture element'.

[SOURCE: IEC 61391-1:2006, 3.23, modified]

3.6

pixel value

integer value of a processed signal level or integer values of processed colour levels, provided to the display for a given **pixel**

Note 1 to entry: In a gray-scale display the pixel value is converted to a luminance by some, usually monotonic, function. The set of integer values representing the gray scale runs from 0 (black) to $2^{(M-1)}$ (white), where *M* is a positive integer, commonly called the bit depth. Thus, if *M* = 8, the largest **pixel value** in the set is 255.

3.7

digitized image data

two-dimensional set of **pixel values** derived from the ultrasound echo signals that form an ultrasound image

3.8

mean pixel value

MPV

mean of **pixel values** detected over an area *A* in a phantom image, where *A* is somewhat smaller than the area of a circle of diameter *D*

Note 1 to entry: The phrase "somewhat less than" is introduced as partial compensation for the partial volume effect in the elevational dimension [3].

Note 2 to entry: The partial volume effect is a term common in CT and MR imaging, namely if an object is smaller than the slice thickness, then the signal will include the contribution of that object and the material around it. For example, if the object is a sphere, then contribution to the signal will occur from material surrounding the sphere

and in a cylinder with radius equal to that of the sphere and perpendicular to the slice. In the ultrasound case, the slice corresponds to the elevational beam profile.

**3.9
depth interval**

interval in depth of area segments into which an image area is subdivided for computation of $LSNR_m$ -values as a function of depth

Note 1 to entry: Experience determining $LSNR_m$ -values for numerous cases has led to the conclusion that a 5 mm-**depth interval** is adequate for the phantoms containing 3,2 mm-diameter and 4 mm-diameter, low-echo spheres, and a 2 mm-**depth interval** is adequate for the phantoms containing 2 mm-diameter, low-echo spheres.

Note 2 to entry: The maximum depth (depth of field) is the sum of a set of contiguous **depth intervals**; thus, if the depth of field is 14 cm and each depth interval spans 5 mm = 0,5 cm, then there are 14 cm/0,5 cm = 28 **depth intervals**.

Note 3 to entry: A rectangular scan area will be subdivided into horizontal bands; a sector scan area will be subdivided into annular ring segments, the angular limits being determined by the sector angle [see Figure B.2 d)]. Rectilinear projection of these area segments in the elevational direction will create volume segments analogous to slabs and partial cylindrical shells with thickness equal to the **depth interval**, respectively.

Note 4 to entry: **Depth interval** is expressed in millimetres (mm).

**3.10
detectability**

numerical value quantifying the probability that a human observer will detect an object in an image having background speckle

**3.11
lesion signal-to-noise ratio for the *n*th low-echo sphere**

$LSNR_n$
numerical value quantifying the **detectability** of a macroscopically uniform, low-echo sphere in a macroscopically uniform, surrounding-background material and having its centre in a volume segment determined by a given **depth interval** in the phantom

Note 1 to entry: Low-echo spheres with centres located less than a distance, $2D$, from a lateral image boundary are excluded.

**3.12
mean lesion signal-to-noise ratio**

$LSNR_m$
mean value of **lesion signal-to-noise ratios** for **low-echo spheres** whose centres lie in a volume segment determined by a given **depth interval** in the phantom

Note 1 to entry: Low-echo spheres with centres located less than a distance, $2D$, from a lateral image boundary are excluded.

4 Symbols

Symbol	Meaning	Clause
A	area in an image plane selected for calculation of MPV	3.8
BSC_{obj}, BSC_{bkg}	backscatter coefficient	3.2
D	low-echo sphere diameter	3.4
d	integer for counting depth intervals	E.1
i, j, k	integers corresponding to rows and columns and the elevational direction of the cubic array, respectively	8.2
i (in Annex F)	index taking values 1 or 2 to indicate one side or opposite side of a phantom, where a reflector is situated	Formula (F.1)

Symbol	Meaning	Clause
$LSNR_m$	mean lesion signal-to-noise ratio	3.12
$LSNR_n$	lesion signal-to-noise ratio for the n th low-echo sphere	3.11
M_d	mean of all $MPVs$ with centres lying within volume segment, d , using the entire image set	E.1
MPV	mean pixel value	3.8
$(MPV)_{ijk}$	MPV at the ijk -site of the cubic array	8.2
$(MPV)_n = S_{Ln}$	MPV calculated over area A centred at the projection of (x_{CMn}, y_{CMn}) onto the image plane nearest to z_{CM}	8.2
N	total number of detected low-echo spheres with centres in the volume segment determined by a depth interval (including all image frames)	8.3.2
n	integer for counting low-echo spheres	3.11
$P(u)$	probability of there being u low-echo sphere centres in an arbitrarily chosen 1 ml volume	6.2.4
q	exponent of the frequency dependence of the backscatter coefficient	6.3
R_i and N_i	mean pixel values on the reflector side and non-reflector side of phantom	Formula (F.1)
$S_{Ln} = (MPV)_n$	MPV calculated over area A centred at the projection of (x_{CMn}, y_{CMn}) onto the image plane nearest to z_{CM}	8.3.2
S_{mBn}	mean of all $MPVs$ in the specified image plane whose centres are within the annulus defined by radii equal to $(3/4)D$ and $2D$ and centred at the coordinates of S_{Ln}	8.3.2
SD_d	standard deviation of all $MPVs$ with centres lying within volume segment, d , using the entire image set	E.1
$x_{CMn}, y_{CMn}, z_{CMn}$	coordinates of the centre of mass of the n th low-echo sphere	E.1
x_n, y_n	projections onto the nearest image plane of the x - and y -coordinates of the centre of mass of the n th low-echo sphere (x_{CMn}, y_{CMn})	8.2
ν	mean number of low-echo sphere centres per millilitre	6.2.4
σ_{Bn}	standard deviation of all $MPVs$ contributing to S_{mBn}	8.3.2

NOTE Additional symbols used only in relation to Figure F.4 are defined in the text below that figure.

5 General and environmental conditions

The manufacturer's specification should allow comparison with the results obtained from the tests described in this Technical Specification.

All measurements should be performed within the following ambient conditions:

- temperature, 23 °C ± 3 °C;
- relative humidity, 10 % to 95 %;
- atmospheric pressure, 66 kPa to 106 kPa.

Properties of ultrasound phantoms, such as speed of sound and attenuation coefficient, can vary with temperature. Consult the specifications published by the phantom manufacturer to determine whether the expected acoustic properties are maintained under the above environmental conditions. If not, the environmental conditions over which expected and reproducible results can be obtained from the phantom or test object should be adopted for tests described below.

6 Equipment required

6.1 General

The test procedures described in this Technical Specification should be carried out using tissue-mimicking phantoms with **digitized image data** acquired from the ultrasound scanner.

6.2 Phantom geometries

6.2.1 Phantoms for use in the frequency range 2 MHz to 7 MHz

The phantom should allow imaging to a depth of at least 16 cm and provide for display of the entire B-scan image frame. Low-echo spheres should be available for **detectability** assessment over the entire image frame and the diameter of these spheres should be specified by the manufacturer within ±1 %. The mean number of spheres per unit volume should be at least 1 per millilitre, but the volume fraction consisting of spheres should not exceed 3,3 %. Scanning windows should provide for contact of the entire emitting surface of the transducer (**active area of a transducer**), while allowing elevational translation of the transducer over a sufficient distance that the most likely number of spheres traversed by the scan plane at or near the focal distance(s) is 25 or more in a 5-mm **depth interval**. A **low-echo sphere diameter** between 3 mm and 4 mm is recommended for adequate performance assessment in the 2 MHz to 7 MHz range.

NOTE One low-echo sphere can serve as two such spheres if total internal reflection at a planar surface provides an independent image. See Annex A for an example of geometry.

6.2.2 Phantoms for use in the frequency range 7 MHz to 15 MHz including "micro-convex" arrays

The phantom should allow imaging to a depth of at least 10 cm and provide for display of the entire B-scan image frame. Low-echo spheres should be available for **detectability** assessment over the entire image frame and the diameter of these spheres should be specified by the manufacturer within ±1 %. The mean number of spheres per unit volume should be at least 8 per millilitre, but the volume fraction consisting of such spheres should not exceed 3,3 %. Scanning windows should provide for contact of the entire emitting surface of the transducer while allowing elevational translation of the transducer over a sufficient distance that the most likely number of spheres traversed by the scan plane at or near the focal distance(s) is 25 or more in a 2 mm-**depth interval**. A **low-echo sphere diameter** between 1 mm and 2 mm is recommended for adequate performance assessment in the 7 MHz to 15 MHz range.

NOTE One low-echo sphere can serve as two such spheres if total internal reflection at a planar surface provides an independent image. See Figure D.1 for an example of geometry.

6.2.3 Total internal-reflection surfaces

For phantoms with low-echo spheres having diameters of 3 mm to 4 mm, two parallel, plate-glass surfaces causing total internal reflection are acceptable in the phantom, as shown in Figures. A.1 and A.2. For phantoms with low-echo spheres having diameters of 1 mm to 2 mm, two parallel, planar, alumina surfaces causing total internal reflection are acceptable in the phantom, as shown in Figure D.1; a surface roughness of the alumina of 6 µm or less is sufficient.

6.2.4 Spatially random distribution of low-echo spheres

Though the positioning of low-echo spheres in the phantom may be precisely defined, manufacturing costs will likely be much lower if the spheres are spatially randomly distributed.

The spatially random distribution of low-echo spheres in a phantom is closely approximated by the Poisson probability distribution function,

$$P(u) = \frac{e^{-\nu} \nu^u}{u!} \quad (1)$$

where

ν is the mean number of low-echo sphere centres per millilitre.

For example, if $\nu = 1$ and $P(u)$ is the probability of there being u low-echo sphere centres in an arbitrarily chosen 1 ml volume, the standard deviation is $\sigma = \nu^{1/2} = 1$.

6.3 Ultrasonic properties of the tissue-mimicking (TM) phantoms

For any phantom, the following ultrasonic property ranges are specified to apply at 23 °C.

NOTE Property values and tolerances specified here are generally similar, but not identical, to those specified in IEC 61391-1:2006 and IEC 61391-2:2010.

Mass density: $(1,05 \pm 0,02)$ g ml⁻¹

Attenuation coefficient divided by the frequency: $(0,50 \pm 0,04)$ dB cm⁻¹ MHz⁻¹ for the low-echo sphere material OR $(0,70 \pm 0,04)$ dB cm⁻¹ MHz⁻¹ for the background material (surrounding the low-echo spheres) AND the value for the low-echo sphere material should be within $0,04$ dB cm⁻¹ MHz⁻¹ of the background value.

Propagation speed: $(1\,540 \pm 10)$ m s⁻¹

Backscatter coefficient for the 2 MHz to 15 MHz case: For the background material 3×10^{-4} (sr cm)⁻¹ ± 3 dB at 3 MHz and frequency dependence of (frequency) ^{q} , where $3 \leq q \leq 4$, and for the low-echo sphere material, no higher than -20 dB relative to the background material.

Long-term stability: With appropriate attention, a phantom should maintain its original values of **backscatter coefficient** within ± 5 dB, attenuation coefficient/frequency within ± 8 %, propagation speed ± 1 % and density ± 2 % for at least 5 years. For water-based tissue-mimicking materials this requirement can be assured *via* periodic monitoring of the phantom weight as specified by the manufacturer. When the weight has decreased by a specified amount, the phantom can be returned to the manufacturer for transfusion with sufficient aqueous solution to return the phantom to its weight (and presumably ultrasonic properties) at the time of manufacture.

7 Data acquisition assuming a spatially random distribution of low-echo spheres

7.1 Methodology

The basic unit for data acquisition for transducer types a) through d) of Clause 1 is a digitized gray-scale image including the entire selected field of view. Typically, at least 8 bits (256 levels) of distinct gray levels are realized. For transducer types e) and f) of Clause 1, see Annex K.

NOTE 1 It is customary that software and hardware will be made available that simplify acquisition, recording and long-term storage of these data.

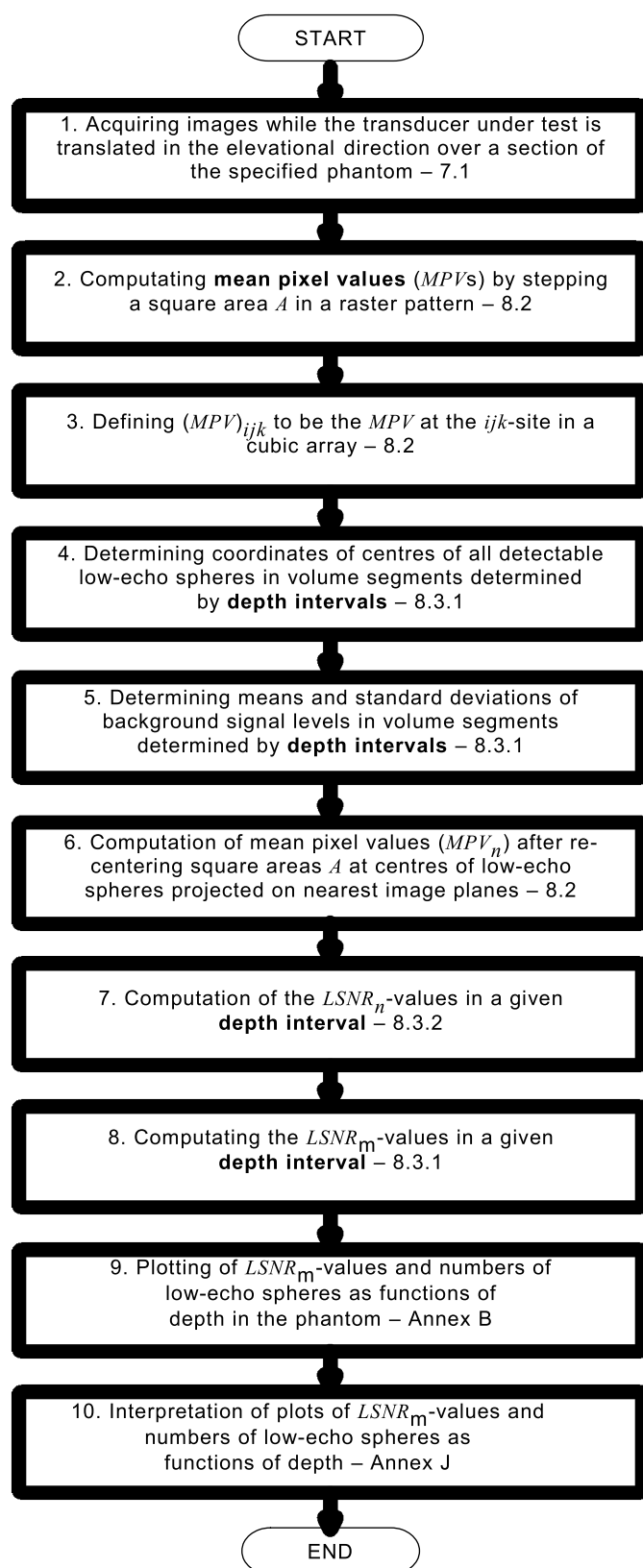
Figure 1 shows a flow chart of the methodology.

The measurement protocol involves acquiring images while the transducer under test is translated in the elevational direction over a section of the specified phantom. For those systems in which the beam axes corresponding to the image frame lie in a plane (defining the "scan plane"), the transducer should be held in contact with a section of the scanning window (with adequate coupling gel) by an apparatus which also allows translation in the elevational direction, thereby allowing acquisition of image frames with scan planes parallel to one another [7].

NOTE 2 Either the transducer or the phantom can be translated.

The maximum translational increment between acquired frames is a function of the low-echo sphere diameter and allows the plane of symmetry (scan plane) of at least one frame to lie within 1/8 of the sphere diameter from the centre of a detected sphere; i.e. the maximum increment should be equal to 1/4 of the sphere diameter.

NOTE 3 If an alternative method for determination of low-echo sphere centres were shown in a peer-reviewed publication to be at least as accurate as the method in Clause 7 and Annex E, and alternative software were also made available for computing $LSNR_m$ -values as a function of depth, which agree with values obtained in reference [7], then employment of such an alternative method would not be in conflict with this Technical Specification.



IEC

Figure 1 – Flow chart

7.2 Storage of digitized image data

Image data in a DICOM (Digital Imaging and Communications in Medicine [8]) format are available on most scanners. Software capable of transferring and opening DICOM-formatted

images is available. When bitmap images are available from the scanner, those also can be used. Factors described in 6.4 of IEC 61391-2:2010 apply.

7.3 Digital image files available from the scanner itself

This method is used by most scanner manufacturers for in-house quality-control testing and image-processing development. Capabilities exist to extend the method for use by clinical personnel using, for example, file-transfer protocol (ftp) resources. Alternatively, many scanners provide image files on removable media, such as USB thumb drives, magneto-optical disks, zip disks, or CD-ROM, and these are appropriate sources of digital image data as well. Full-screen capture is available on many systems.

7.4 Image archiving systems

Many imaging centres use commercially available Picture Archiving and Communication Systems (PACS) for viewing and storing ultrasound image data. Manufacturers of PACS systems usually provide means to acquire images in an uncompressed format, such as a 'tiff' (Tagged Image File Format) or a DICOM (Digital Imaging and Communications in Medicine [8]) format, by workstations that have access rights to the image data.

8 Automated data analysis for quantifying low-echo sphere detectability

8.1 General

Using the image data obtained as described in Clause 7 and assuming negligible gradients in background *MPVs*, the human-observer-related **detectability** equals the **mean lesion signal-to-noise ratio** ($LSNR_m$) in each one of contiguous volume segments determined by the **depth intervals** spanning the entire depth range available [3], [7].

Recall from Clause 3.11 that the **lesion signal-to-noise ratio for the *n*th low-echo sphere** ($LSNR_n$) is a numerical value quantifying the **detectability** of a macroscopically uniform, low-echo sphere in a macroscopically uniform, surrounding-background material, with its centre lying in a volume segment determined by a given **depth interval**. Low-echo spheres and background material have **intrinsic backscatter coefficients**, namely, BSC_{obj} and BSC_{bkg} , respectively. For a spherical inclusion, $LSNR_n$ has been defined and discussed extensively [9].

NOTE The "object contrast" in decibels equals $10 \log_{10} [BSC_{obj}/BSC_{bkg}]$, and this value is -20 dB or lower for the low-echo spheres in comparison to background material in the specifications above. Subscripts L ("Lesion") and B ("Beads") are special cases of subscripts "obj" and "bkg", respectively.

8.2 Computation of mean pixel values (*MPVs*)

MPV, as defined in 3.8, is the mean of pixel values detected over an area *A* in a phantom image, where *A* is somewhat smaller than the area of a circle of diameter *D*; this definition allows for partial compensation for the partial volume effect in the elevational dimension [3].

In this Technical Specification *A* is a square with side $2D/3$ [3]. For each image obtained according to 7.1, a set of *MPVs* is computed over areas *A*, stepped in a raster pattern in the image plane, with centres comprising a simple, square array and nearest neighbour spacing of $D/4$. Thus, for all images obtained by translating the transducer under test in the elevational direction in successive steps of $D/4$, each *MPV* in a set is associated with one of the sites in a simple cubic array.

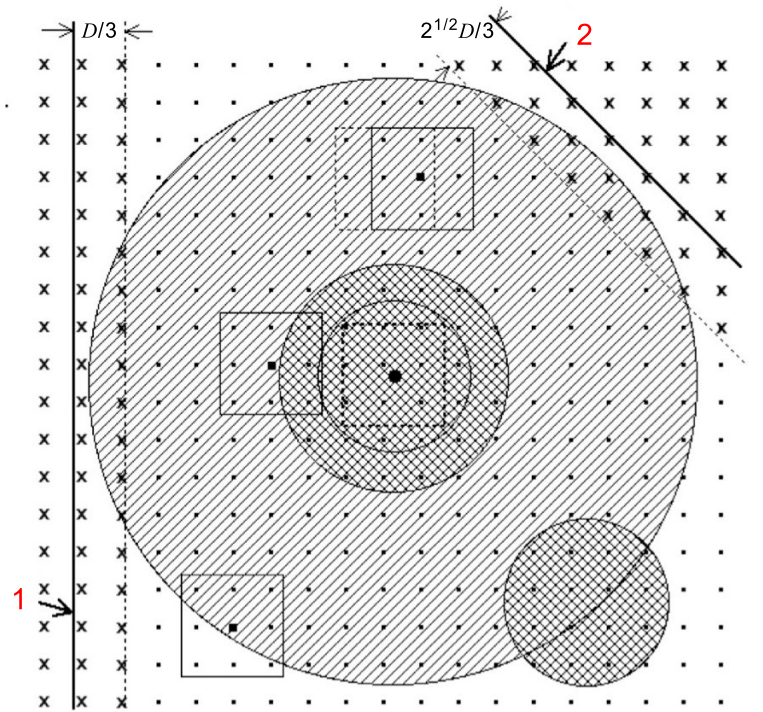
Define $(MPV)_{ijk}$ to be the *MPV* at the *ijk*-site, where *i*, *j* and *k* are integers and $(D/4)i$ is the *x*-coordinate value, $(D/4)j$ is the *y*-coordinate value, and $(D/4)k$ is the *z*-coordinate value of the site. Also, *i* and *j* correspond to rows and columns, and *k* to the elevational direction, respectively, of the cubic array.

Next, the coordinates $(x_{CM}, y_{CMn}, z_{CMn})$ of the centres of low-echo spheres should be determined (see first paragraph in 8.3.1 and E.1). Then, for each n , the **mean pixel value** in the image plane nearest to the n th **low-echo sphere** centres for the site having x - and y -coordinates equal to those of the centre $(x_{CMn}$ and $y_{CMn})$ is computed, giving rise to a new set of MPV -values (MPV_n , also designated as the signal S_{Ln}); in general, these x_n - and y_n -coordinates will not coincide with the coordinates of any $(MPV)_{ijk}$. When computing these MPV_n , the only significant **pixels** lie within the inner circle shown in Figure 2; therefore the cross-hatching, which otherwise denotes an exclusion zone, does not apply to computations of MPV_n . See also Formula (2) regarding the role of S_{Ln} .

Figure 2 is a schematic of an image plane showing the special case of an in-plane, low-echo sphere centre (●), concentric circles of radii defined in 8.3, and examples of stepping square areas A , delineated for computing **mean pixel values** $(MPV)_{ijk}$ that are assigned to the array sites (■) centred in each square.

In Figure 2 $MPVs$ at image-plane sites in the central cross-hatched area are excluded from calculations of the background means and standard deviations, while $MPVs$ at image-plane sites in the diagonally hatched annulus are included, unless they are within a sphere of radius $3D/4$ concentric with a different low-echo sphere centre (e.g. at lower right) or are within limits (dashed lines) adjacent to a linear-array or sector-scan image boundary (vertical or oblique, full lines, respectively) – 8.3.1.





Key

- (MPV)-array sites (i,j,k) in the image plane with grid-spacing D/4 – Clause 7
- nth low-echo sphere centre, which is also in the image plane in this special case:

$$(x = x_{CMn}, y = y_{CMn}, z = z_{CMn}); \text{ in general } (x \neq x_{CMn}, y \neq y_{CMn}, z \neq z_{CMn})$$

The inner circle is a **low-echo sphere** boundary (physical), having (special-case) radius D/2 at its intersection with the image plane; in general the intersection radius is $\leq D/2$ – see 3.4.

The middle circle (mathematical) in the image plane has (special-case) radius 3D/4; in general the intersection radius is $\leq 3D/4$ – see 8.3.1.

The outer circle (mathematical) in the image plane has (special-case) radius 2D; in general the intersection radius is $\leq 2D$ – see 8.3.2.

The full-line squares (examples) denote areas A in the image plane, having sides of length 2D/3 and used to compute (MPV)_{ijk}-values that are assigned to the array sites (■) at the centres of those squares – see 8.2; when circles intersect such squares, software makes choices to include or exclude some pixels (cross-hatching indicates an exclusion zone) – see 8.3.

The dashed-line square (top) denotes the previous, stepped area A in the image plane for computing (MPV)_{ijk} – see 8.2.

The dotted-line square (centre) denotes area A in the image plane for computing MPV_n (exclusion and cross-hatching are not applicable) – see 8.3.2.

The circular cross-hatched area (lower right) has radius $\leq 3D/4$ and denotes the intersected area of the image plane with the “middle circle (mathematical)” surrounding another, out-of-plane, low-echo sphere, having its centre at $z \neq z_{CMn}$ – see 8.3.1.

- 1 Vertical, full line and parallel dashed line denote the lateral boundary of a linear-array image and the boundary of the exclusion zone of breadth D/3 identified by crosses (X).
- 2 Oblique, full line and parallel dashed line denote the lateral boundary of a sector-scan image and the boundary of the exclusion zone of breadth 2^{1/2}D/3 identified by crosses (X); the chosen breadth of the exclusion zone is dependent on the sector angle and the specific breadth for a 90°-sector is shown.

Also X denotes a square array site that does not have an associated (MPV)_{ijk} and therefore does not contribute to calculations of S_{mBn} or σ_{Bn} in Formula (2).

Figure 2 – Schematic of an image plane

8.3 Determination of the $LSNR_m$ -value for a given depth interval

8.3.1 Preliminaries

Firstly, the Cartesian coordinates of the centres of all detectable low-echo spheres in the volume segment determined by the **depth interval** should be determined. A preferred method for accomplishing this is described in Clause 7 and Annex E, and this is also the method used in determining $LSNR_m$ -values as a function of depth in other annexes.

Secondly, all $MPVs$ that might be significantly influenced by the presence of a neighbouring low-echo sphere should be eliminated *for computation of background means and standard deviations* in subclause 8.3.2; that is, for this computation, do not use any MPV_{ijk} at cubic array sites that lie within a radius equal to $3D/4$ of *any* low-echo sphere centre, the coordinates of which were determined according to the last paragraph above.

8.3.2 Computation of the $LSNR_n$ -values and $LSNR_m$ -value in a given depth interval

The $LSNR_n$ for the n th low-echo sphere is defined by

$$LSNR_n = \frac{(S_{L_n} - S_{mB_n})}{\sigma_{B_n}} \quad (2)$$

where, in terms of the coordinates of low-echo sphere centres as determined in Annex E [7],

S_{L_n} is an MPV (called MPV_n in last paragraph of 8.2) with x - and y -coordinates equal to x_{CM_n} and y_{CM_n} , respectively, for the n th sphere and z (elevational) coordinate corresponding to the image plane closest to z_{CM_n} .

S_{mB_n} is the mean of all $MPVs$ in the specified image plane whose centres are within the annulus defined by radii equal to $3D/4$ and $2D$ and centred at the coordinates of S_{L_n} ; see 8.3.1 and Figure 2 for geometric clarity.

σ_{B_n} is the standard deviation of all $MPVs$ contributing to S_{mB_n} .

The $LSNR_m$ -value for the volume segment determined by the **depth interval** is then

$$LSNR_m = \frac{1}{N} \sum_{n=1}^N LSNR_n \quad (3)$$

where

N is the total number of detected low-echo spheres with centres in the volume segment determined by the depth interval (including all image frames) but excluding those lying within $2D$ of a phantom boundary (see 3.11).

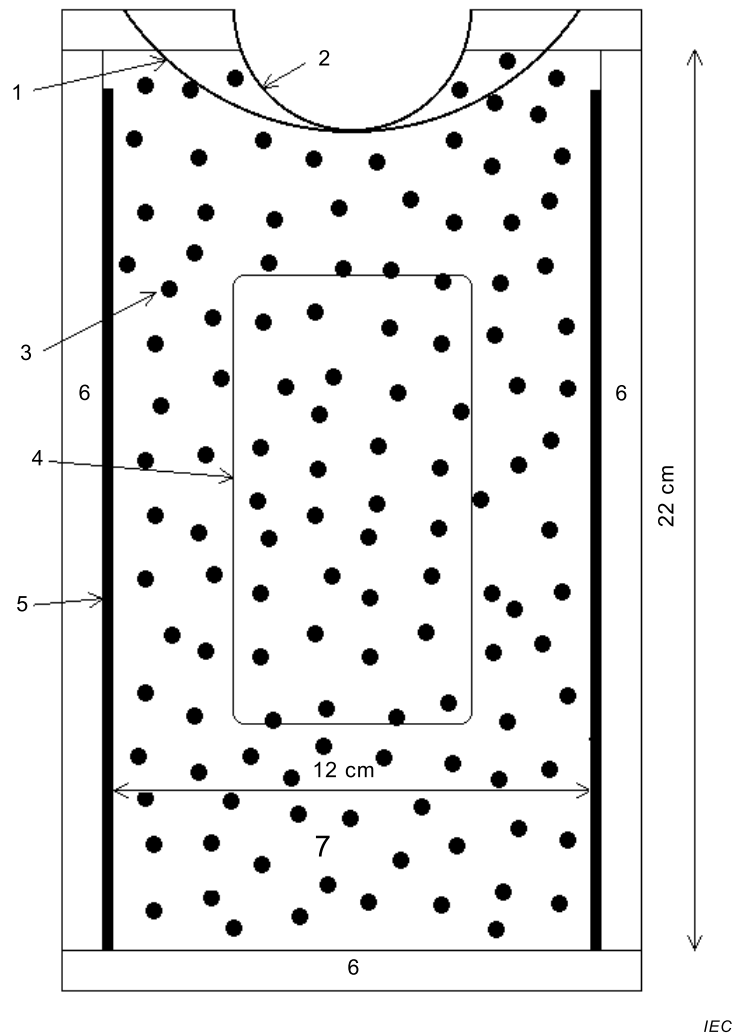
8.3.3 Standard error corresponding to each $LSNR_n$ -value

The standard error corresponding to each $LSNR_n$ -value is given by $N^{-1/2}$ times the standard deviation of the $LSNR_n$ -values corresponding to the **depth interval** involved.

Annex A (informative)

Example of a phantom for performance testing in the 2 MHz to 7 MHz frequency range

Figures A.1 and A.2 below illustrate a phantom containing low-echo spheres that meets the specifications in this Technical Specification. Figure B.1 shows an image of a prototype phantom having nearly the same dimensions as are depicted in Figures A.1 and A.2. A flat alumina reflector exists in place of one of the plate glass reflectors. The alumina reflector has a slightly rough surface, giving rise to diffuse echoes at its surface.

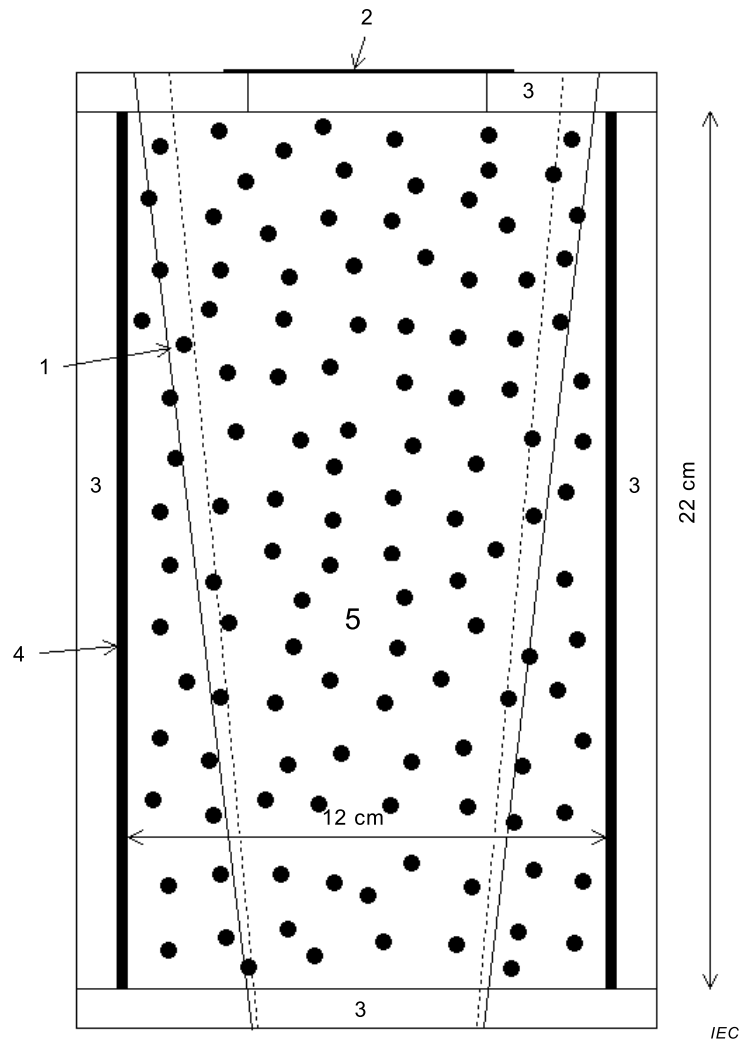


Key

1	7 cm radius of curvature scan window at TM material boundary
2	3 cm radius of curvature scan window at TM material boundary
3	anechoic sphere
4	6 cm × 11 cm flat scanning window
5	plate-glass reflector
6	1 cm thick acrylic plate
7	background material with speed of sound = 1 540 m s ⁻¹ and (attenuation coefficient)/frequency = 0,5 dB cm ⁻¹ MHz ⁻¹ and one 4 mm diameter, anechoic sphere per millilitre

Figure A.1 – End view of the phantom applicable for 2 MHz to 7 MHz showing the spatially random distribution of 4-mm diameter low-echo spheres

In Figure A.1 the ends of a conical scanning window are depicted at the top of the phantom. The flat, scanning window accommodates linear arrays, phased arrays and flat 2-D arrays [2]. The parallel plate-glass rectangles provide – via total internal reflection – for extension of the image outside of the volume occupied by tissue-mimicking material.



Key

1	anechoic sphere
2	6 cm × 11 cm flat scanning window
3	1 cm thick acrylic plate
4	plate-glass reflector
5	background material with speed of sound = 1 540 m s ⁻¹ and (attenuation coefficient)/frequency = 0,5 dB cm ⁻¹ MHz ⁻¹ and one 4 mm diameter, anechoic sphere per millilitre

Figure A.2 – Top view of phantom with 4 mm-diameter, low-echo spheres

Annex B (informative)

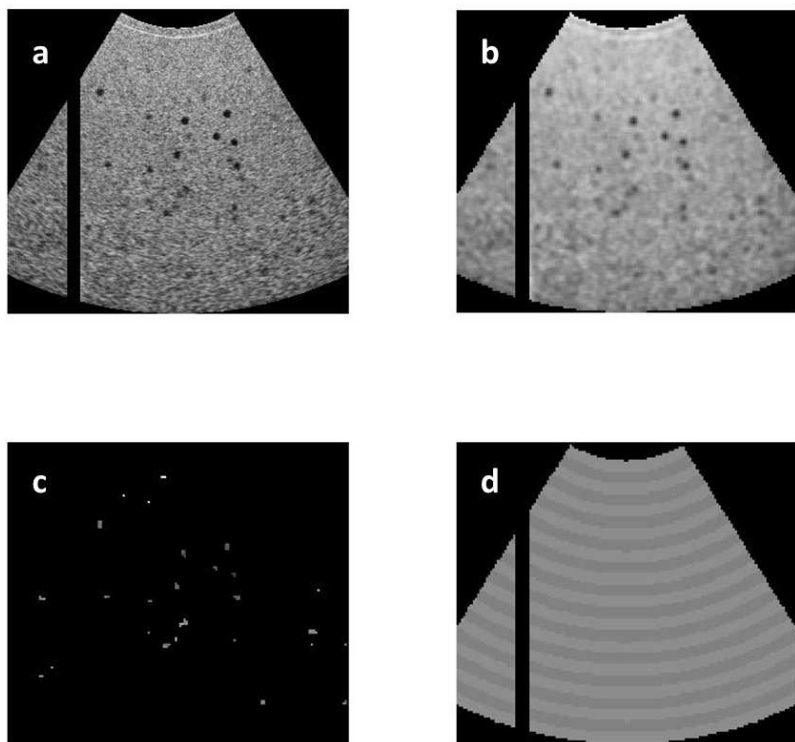
Illustrations of the computation of $LSNR_m$ -values as a function of depth



Figure B.1 – Convex-array image of a prototype 4 mm-diameter low-echo sphere phantom for use in the 2 MHz to 7 MHz frequency range

In Figure B.1 one of the plane reflectors (on the left) is alumina instead of plate glass and a vertical line of elevated echoes occurs at the slightly rough surface of that alumina plate. A parallel, 3 mm-thick, plate-glass reflector exists 10 cm to the right of the alumina plate. The maximum width of the sector image is 18,6 cm. Rigorous testing for the effectiveness of either plate glass or alumina plates, regarding total internal reflection and the effect of surface diffuse scattering, is presented in Annex F.

Figures B.2 through B.8 show auxiliary images, and results of analysis, as described in more detail in the figure and sub-figure captions.

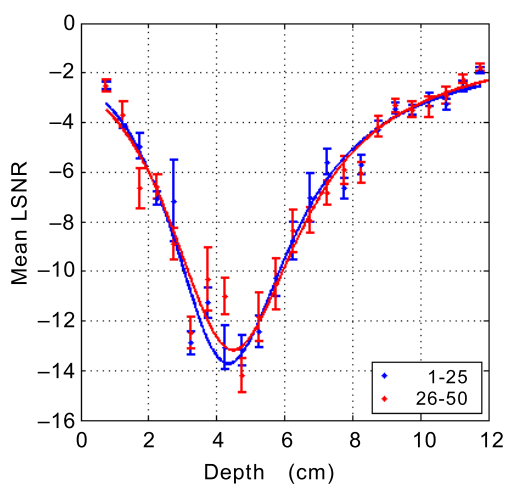


IEC

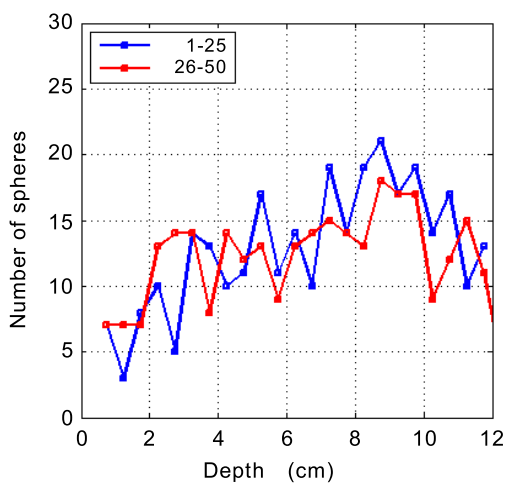
- a) Cropped image from Figure B.1 with the vertical line of low-level, diffuse echoes at the flat, alumina plate's surface removed
- c) Sets of 7 sites identified with a low-echo sphere centre in Figure B.1

- b) Mapping of *MPVs* in gray-scale
- d) 5 mm-depth intervals distinguished with different gray levels

Figure B.2 – Auxiliary figures relating to Figure B.1



IEC



IEC

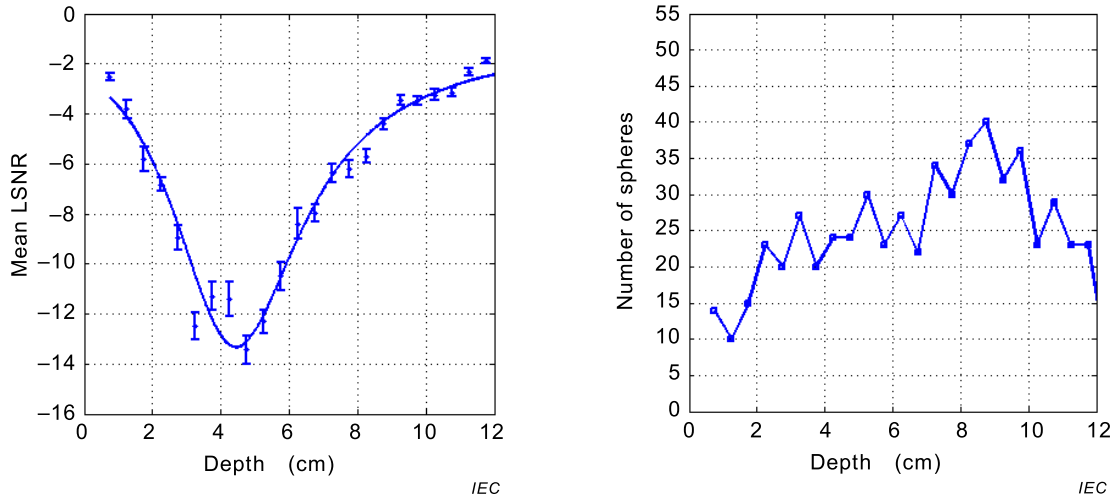
- a) Mean LSNR ($LSNR_m$)-values as a function of depth as determined with two independent sets of 25 images corresponding to Figures B.1 and B.2

- b) Number of low-echo sphere centres detected in each 5 mm-depth interval

In the notation adopted in 8.3.2, read $LSNR_m$ for Mean LSNR at the ordinate label of the left graph.

Figure B.3 – Results corresponding to Figures B.1 and B.2, demonstrating reproducibility

In Figure B.4 a) all 50 images are used in one set; such use is recommended. Figure B.4 b) shows that the number of low-echo spheres in the 5 mm-depth intervals in the focal range is about 25.



a) Mean LSNR ($LSNR_m$)-values as a function of depth using all 50 images corresponding to those in Figure B.3

b) Number of low-echo sphere centres detected in each 5 mm-depth interval

In the notation adopted in 8.3.2, read $LSNR_m$ for Mean LSNR at the ordinate label of the left graph.

Figure B.4 – Results corresponding to Figures B.1, B.2 and B.3



Figure B.5 – One of 80 parallel linear-array images of the phantom containing 4 mm-diameter, low-echo spheres, at 4 MHz with focus at 3 cm

In Figure B.6 the green x's identify the determined centres of the low-echo spheres identified with the respective images. Where there is no x, the low-echo sphere centre was identified with a nearby image.

In Figure B.7 the image set 1 to 40 is independent of the image set 41 to 80. The agreement for the two sets of data plotted in panel a) is reasonable but should be better. Panel b) shows the mean number of **low-echo spheres** in a depth interval is about 7.

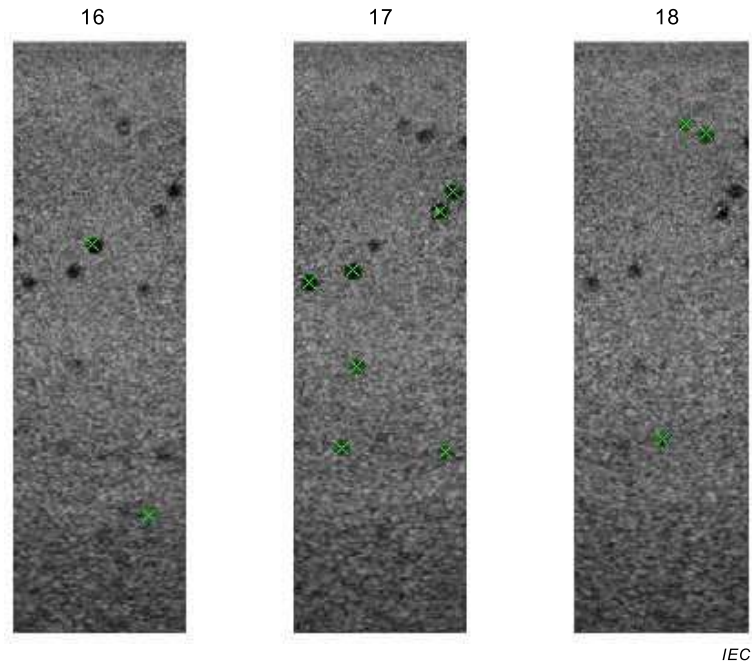
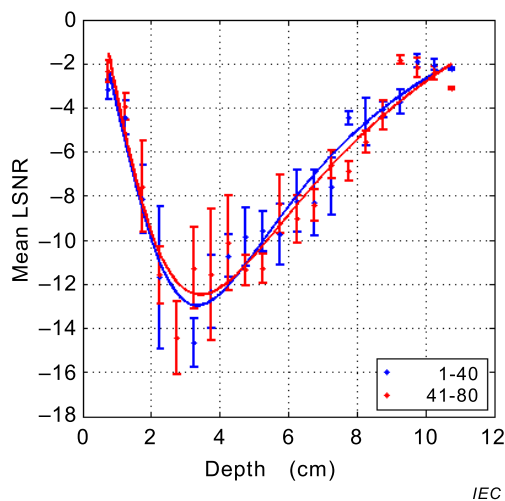
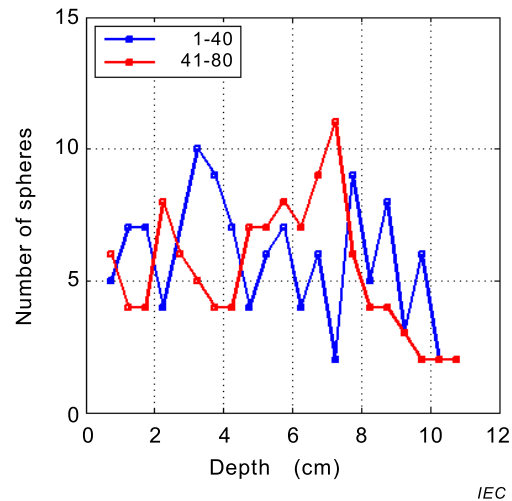


Figure B.6 – Three successive images of the set of 80, separated by $D/4$ equal to 1 mm



a) Mean LSNR ($LSNR_m$)-values as a function of depth



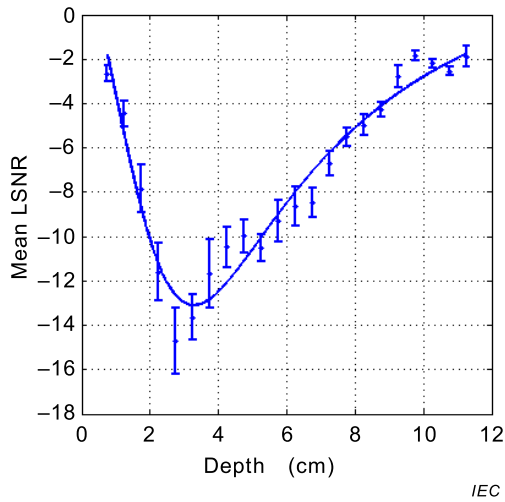
b) The number of low-echo spheres detected in each 5 mm-depth interval

In the notation adopted in 8.3.2, read $LSNR_m$ for Mean LSNR at the ordinate label of the left graph.

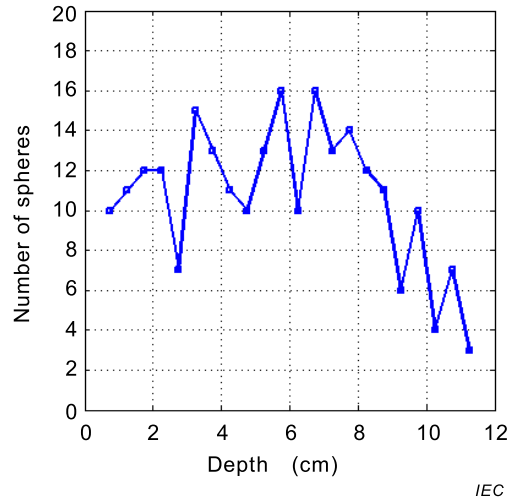
Figure B.7 – Results for the 4 cm-wide, 3 cm-focus, linear array addressed in Figures B.5 and B.6

In Figure B.8 a) the curve-fit is much better for the doubling of the number of **low-echo spheres** per centimetre depth interval. Doubling the number of detected **low-echo spheres** in

the 3 cm-focal zone would better define the minimum (most negative) value of the $LSNR_m$, but the limited area of the window in this phantom precluded obtaining more than 80 images.



a) Mean LSNR ($LSNR_m$)-values as a function of depth



b) The number of low-echo spheres detected in each 5 mm-depth interval is shown

In the notation adopted in 8.3.2, read $LSNR_m$ for Mean LSNR at the ordinate label of the left graph.

Figure B.8 – Results for the 4 cm-wide, 3 cm-focus, linear array addressed in Figures B.5, B.6 and B.7, using all 80 image frames corresponding to Figure B.7

Annex C (informative)

Sufficient number of data images to assure reproducibility of results

C.1 General

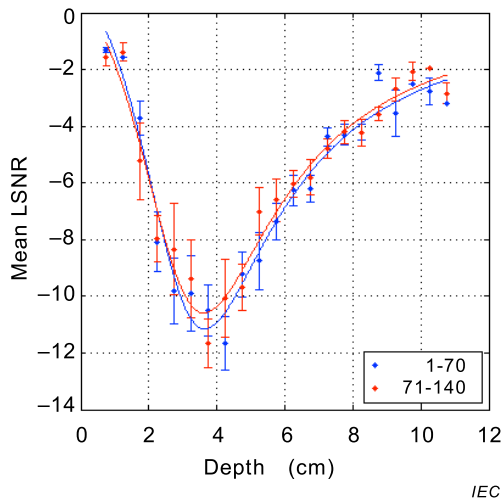
In Annex C evidence is given that the minimum number of data images needed to assure adequate accuracy of $LSNR_m$ -values is about 25 in the focal zone. Reproducibility using independent (non-overlapping) parts of the phantom is assessed.

C.2 Phantom with low-echo sphere diameter 3,2 mm, having 2 spheres per millilitre

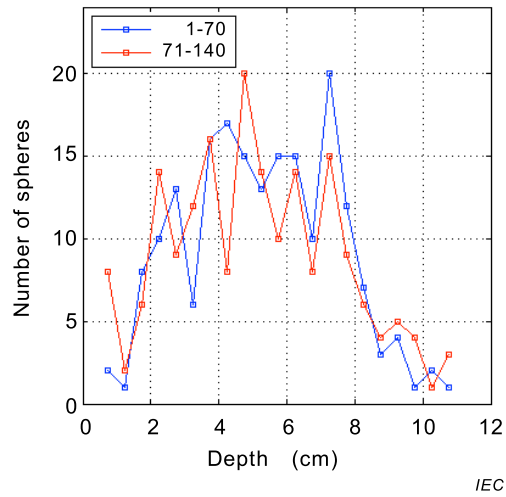
The first example is for a linear array operating at 4 MHz with a focus at 3 cm. The elevational interval between images is $D/4 = 3,2 \text{ mm}/4 = 0,8 \text{ mm}$. An image is shown in Figure C.1. Results for two cases in which there is no overlap between imaged volumes are shown in Figure C.2. Both sets contain 70 images corresponding to a net elevational displacement of $70 \times 0,8 \text{ mm} = 5,6 \text{ cm}$. Here the mean number of low-echo sphere centres per 5 mm-**depth interval** is about 15, instead of 25, but reproducibility is still good. Figure C.3 shows the result when the entire 140 images are used and the average number of low-echo sphere centres per volume segment determined by the **depth interval** is about 30; the curve fit is excellent indicating excellent reproducibility. The net elevational displacement is $140 \times 0,8 \text{ mm} = 11,2 \text{ cm}$.



Figure C.1 – One image obtained from a phantom containing 3,2 mm-diameter, low-echo spheres by using a 4 MHz linear array focused at 3 cm



a) Mean LSNR ($LSNR_m$)-values as a function of depth

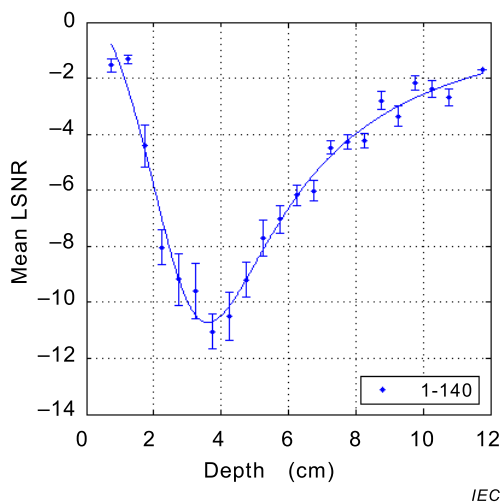


b) Number of low-echo sphere centres detected in each 5 mm-depth interval

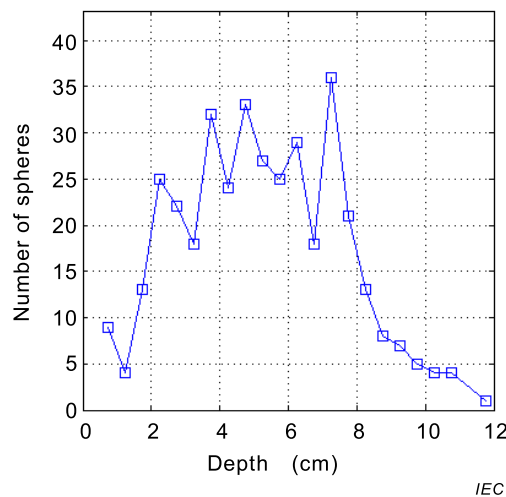
In the notation adopted in 8.3.2, read $LSNR_m$ for Mean LSNR at the ordinate label of the left graph.

Figure C.2 – Reproducibility result for two independent sets of 70 images with a mean number of low-echo sphere centres that is about 15 per 5 mm-depth interval

In Figure C.3 b) the number low-echo spheres per 5 mm-depth interval at the focal depth is about 25, corresponding to the recommended number in 6.2.1, and the curve-fit in a) is good, as expected.



a) Mean LSNR ($LSNR_m$)-values as a function of depth



b) Number of low-echo sphere centres detected in each 5 mm-depth interval

In the notation adopted in 8.3.2, read $LSNR_m$ for Mean LSNR at the ordinate label of the left graph.

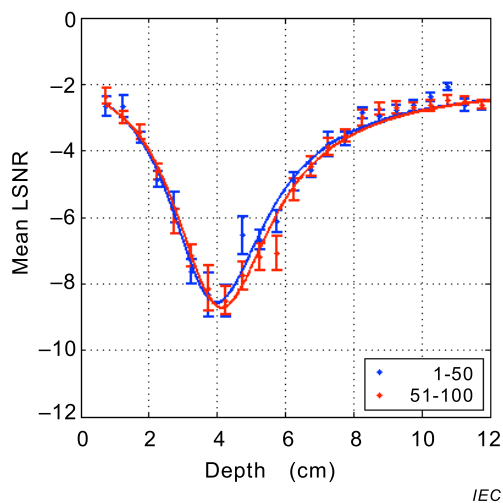
Figure C.3 – Results obtained by using both sets of 70 independent images corresponding to Figure C.2

The next reproducibility study involves a convex array operating at 4,5 MHz and illustrates the ability to differentiate performance for different focusing choices. Figure C.4 shows an image with multiple foci at 4 cm, 8 cm and 12 cm; Figure C.5 shows the corresponding reproducibility results. Figure C.6 shows reproducibility results corresponding to a single, deep focus at 10 cm, whereas Figure C.7 corresponds to a single, shallow focus at 4 cm.

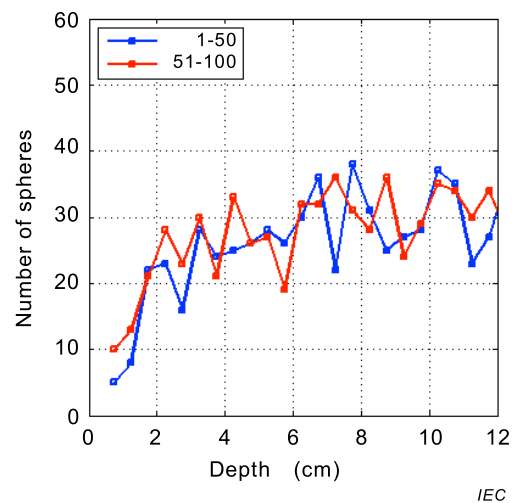


Figure C.4 – Sector image (curved array) at 4,5 MHz with multiple foci at 4 cm, 8 cm and 12 cm depths; the low-echo spheres are 3,2 mm in diameter

In Figure C.5 a) reproducibility is excellent at a mean number of low-echo sphere centres per 5 mm-depth interval of 25. The lateral focusing at 8 cm and 12 cm is barely evident, focusing presumably being strongly dominated by fixed elevational focusing at about 4 cm depth.



a) Mean LSNR ($LSNR_m$)-values as a function of depth

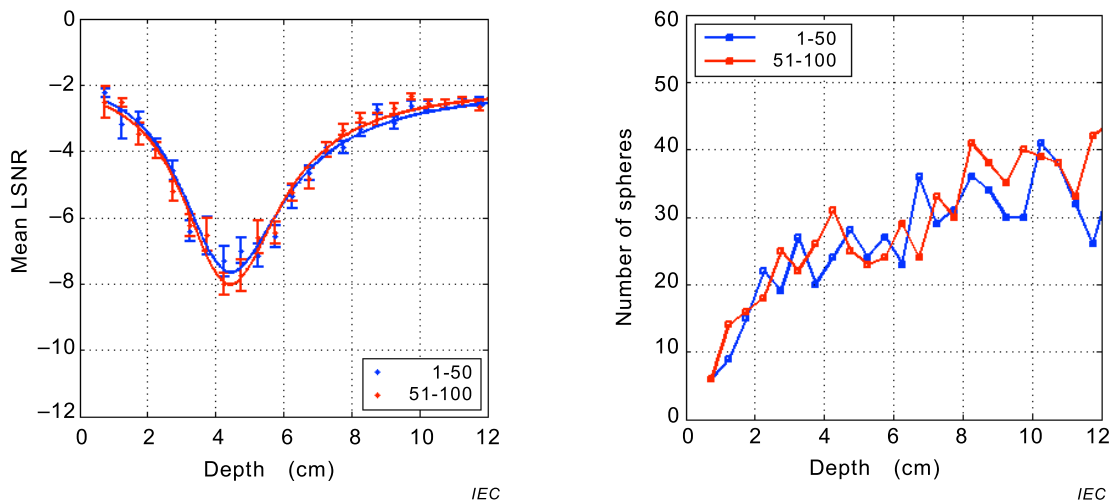


b) The number of low-echo spheres detected in each 5 mm-depth interval

In the notation adopted in 8.3.2, read $LSNR_m$ for Mean LSNR at the ordinate label of the left graph.

Figure C.5 – Reproducibility results for a multiple-lateral-focus (4 cm, 8 cm and 12 cm) case corresponding to Figure C.4

In Figure C.6 a) reproducibility is excellent at a mean number of low-echo sphere centres per 5 mm-depth interval of 25. The lateral focusing at 10 cm is not evident, focusing presumably being strongly dominated by fixed elevational focusing at about 4 cm depth. Notice that there is a distinction between these results and the multiple-focus case in Figure C.5, namely a shallower minimum of $LSNR_m$ at about $-7,9$ instead of about $-8,7$ for the multiple-focus case.



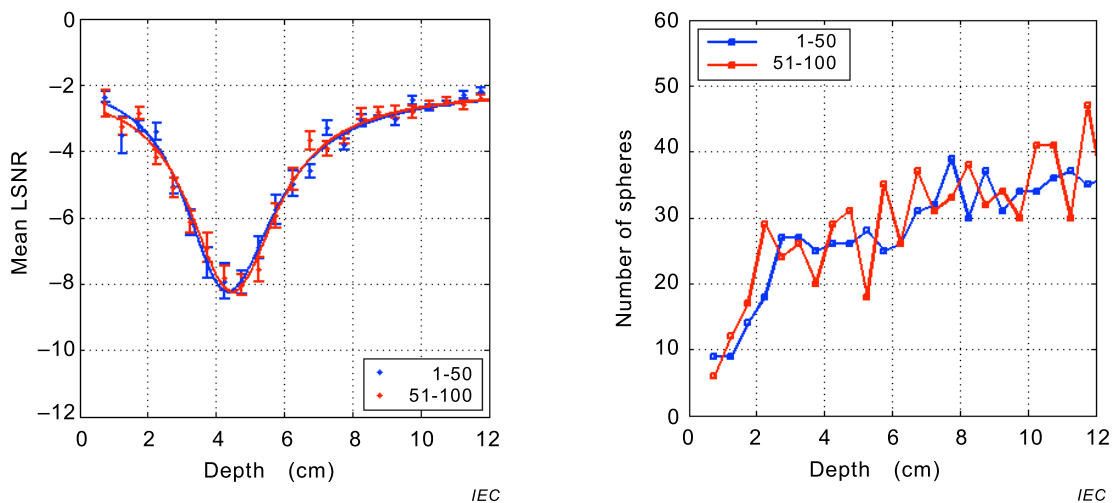
a) Mean LSNR ($LSNR_m$)-values as a function of depth

b) Number of low-echo sphere centres detected in each 5 mm-depth interval

In the notation adopted in 8.3.2, read $LSNR_m$ for Mean LSNR at the ordinate label of the left graph.

Figure C.6 – Reproducibility results for the case corresponding to Figure C.5, except that there is a single focus at 10 cm depth

In Figure C.7 a) reproducibility is excellent at a mean number of low-echo sphere centres per 5 mm-depth interval of 25. The 10 cm- and 4 cm-focus cases are almost indistinguishable, the 4 mm case having a slightly deeper minimum (negative value).



a) Mean LSNR ($LSNR_m$)-values as a function of depth

b) Number of low-echo sphere centres detected in each 5 mm-depth interval

In the notation adopted in 8.3.2, read $LSNR_m$ for Mean LSNR at the ordinate label of the left graph.

Figure C.7 – Reproducibility results for the case corresponding to Figure C.5, except that there is a single focus at 4 cm depth

C.3 Phantom with 2 mm-diameter, low-echo spheres and 8 spheres per millilitre

Figure C.8 shows an image of the phantom containing 2 mm-diameter, low-echo spheres, made with a curved array having 1,5 cm radius of curvature, with its focus at 3 cm. The C8-5 transducer designation implies that the pulse spectrum lies in the 5 MHz to 8 MHz range.

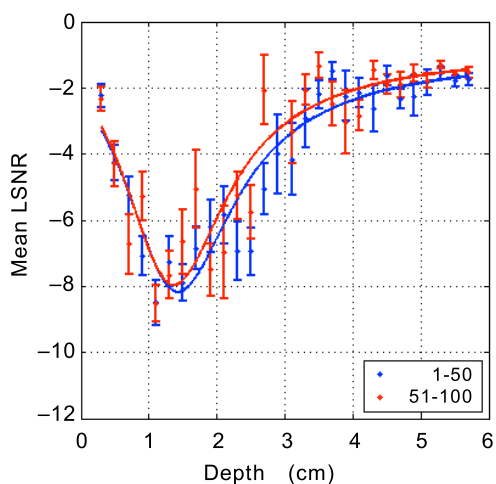


IEC

Figure C.8 – Image of the phantom containing 2 mm-diameter, low-echo spheres, made with a curved array having 1,5 cm radius of curvature, with its focus at 3 cm

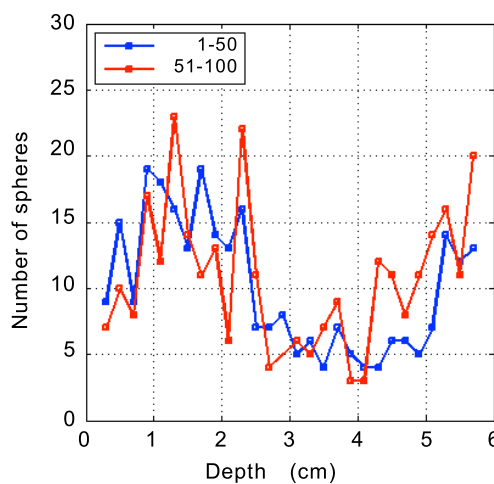
Figures C.9 and C.10 show corresponding reproducibility results. (See Annex D for diagrams of this phantom.)

Although $LSNR_m$ reproducibility is reasonable in Figure C.9 a), the plotted points are spread more than desired and error bars are rather large. Images 1 to 50 are independent of images 51 to 100. Note from panel b) that the number of low-echo spheres detected per 2 mm-depth interval in the focal range is about 15, which is fewer than the recommended minimum of 25.



IEC

a) Mean LSNR ($LSNR_m$)-values as a function of depth



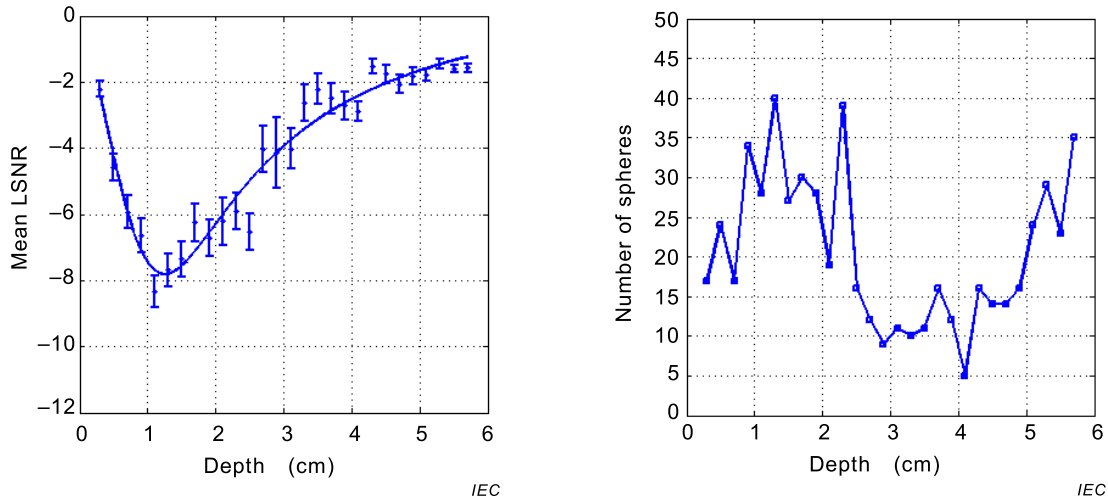
IEC

b) Number of low-echo sphere centres detected in each 2 mm-depth interval

In the notation adopted in 8.3.2, read $LSNR_m$ for Mean LSNR at the ordinate label of the left graph.

Figure C.9 – Reproducibility results corresponding to Figure C.8

In Figure C.10 a) the number of low-echo spheres per depth interval in the focal region (1 cm to 1,5 cm depth range) is about 30. The number of detected, low-echo spheres per 2 mm-depth interval in the depth range 2,5 cm to 3,5 cm is less than 20, compromising the accuracy in that range.



a) Mean LSNR ($LSNR_m$)-values as a function of depth

b) Number of low-echo sphere centres detected in each 2 mm-depth interval

In the notation adopted in 8.3.2, read $LSNR_m$ for Mean LSNR at the ordinate label of the left graph.

Figure C.10 – Results using all 100 images in the image set that gave rise to Figure C.9

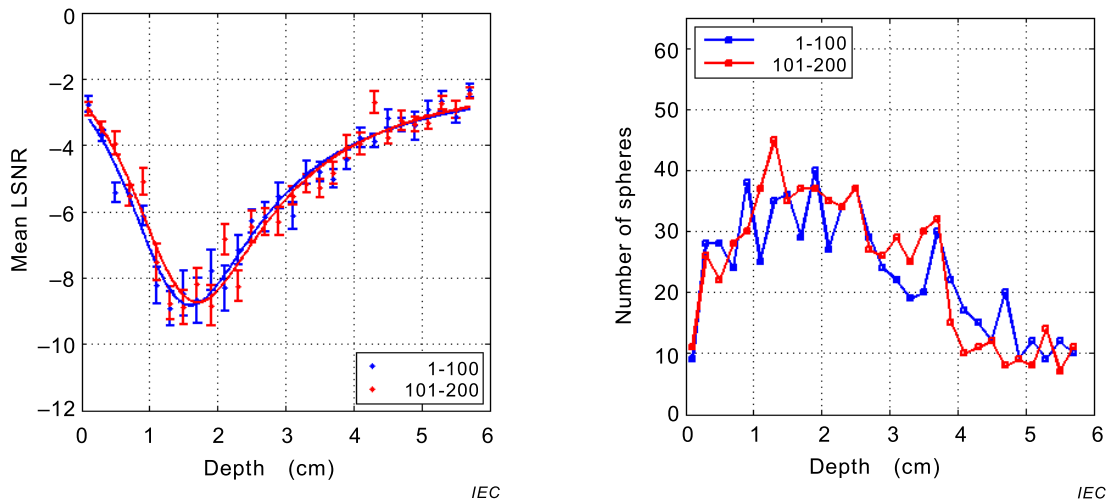
Figure C.11 shows an image of the phantom containing 2 mm-diameter, low-echo spheres, made with a high-frequency (15 MHz) linear array, laterally focused at 4 cm. Figures C.12 and C.13 show corresponding reproducibility results.



IEC

Figure C.11 – Image of the phantom containing 2 mm-diameter, low-echo spheres, made with a high-frequency (15 MHz) linear array, laterally focused at 4 cm

In Figure C.12 a) images 1 to 100 are independent of images 101 to 200. Reproducibility is demonstrated with about 35 detected low-echo spheres per 2 mm-depth interval in the focal-depth range, which again is at the elevational focus of about 1,5 cm.



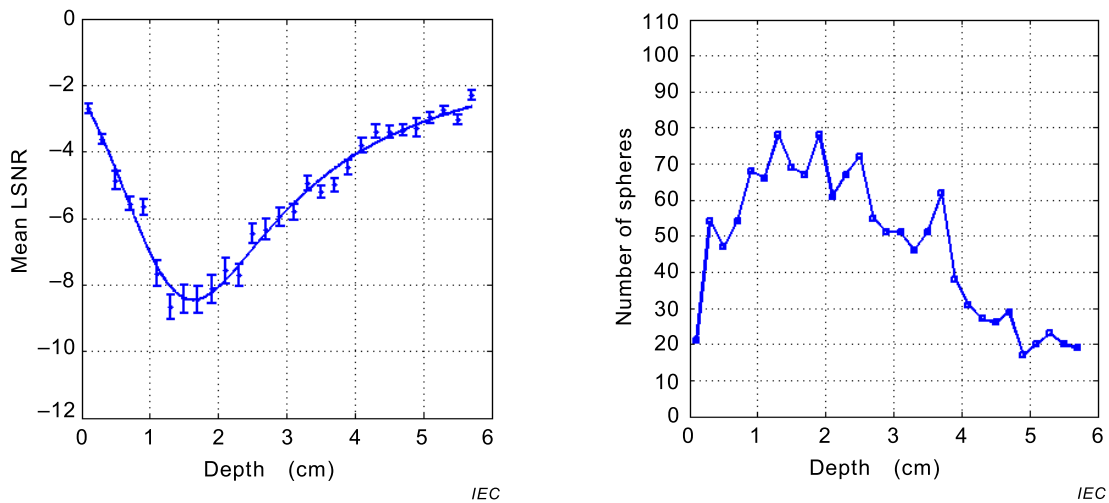
a) Mean LSNR ($LSNR_m$)-values as a function of depth

b) Number of low-echo sphere centres detected in each 2 mm-depth interval

In the notation adopted in 8.3.2, read $LSNR_m$ for Mean LSNR at the ordinate label of the left graph.

Figure C.12 – Reproducibility results corresponding to Figure C.11

In Figure 13 b) the number of low-echo spheres per 2 mm-depth interval in the focal region (1 cm to 1,5 cm depth range) is about 70.



a) Mean LSNR ($LSNR_m$)-values as a function of depth

b) Number of low-echo sphere centres detected in each 2 mm-depth interval

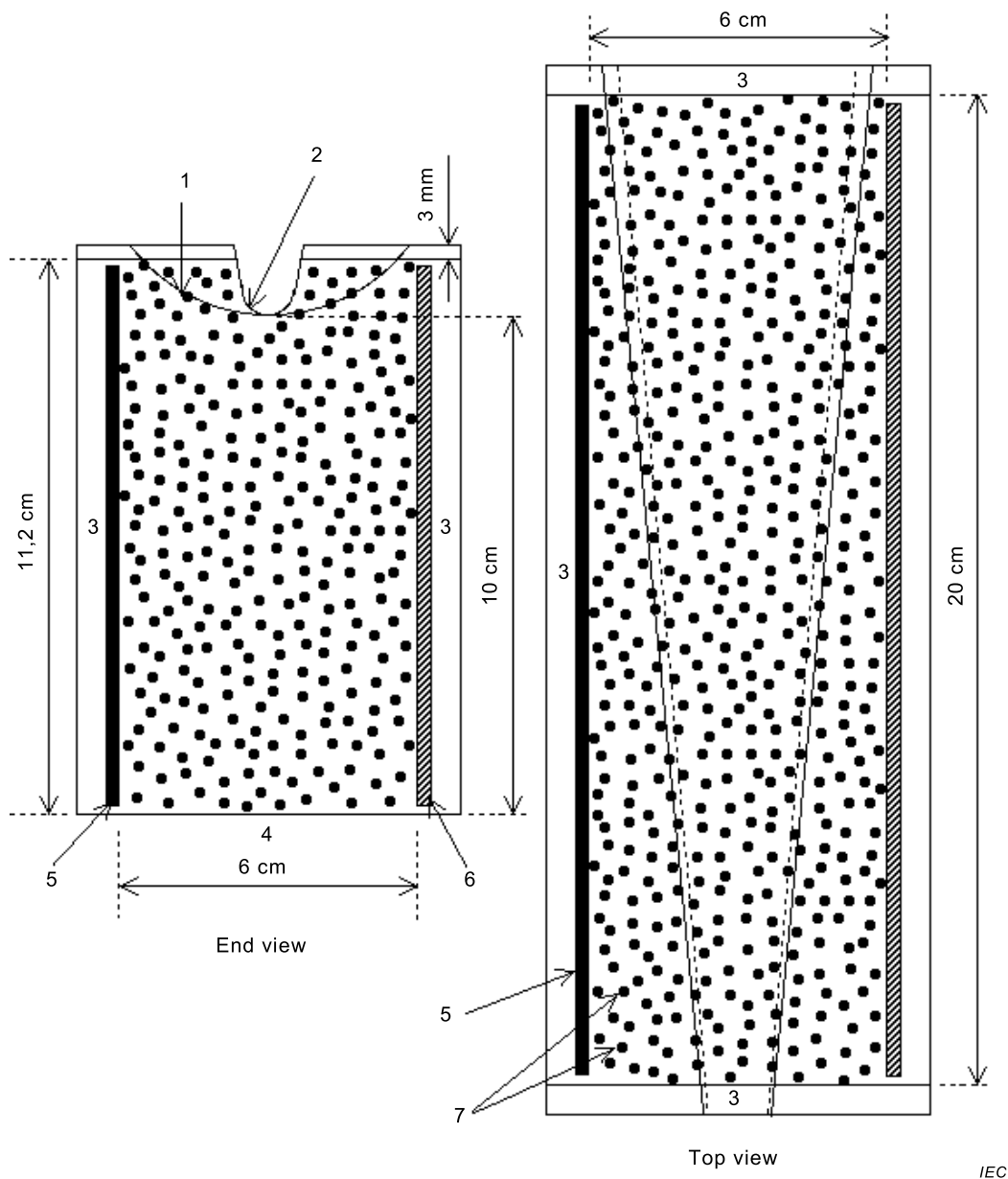
In the notation adopted in 8.3.2, read $LSNR_m$ for Mean LSNR at the ordinate label of the left graph.

Figure C.13 – Results using all 200 images in the image set that gave rise to Figure C.12

Annex D
(informative)

**Example of a phantom for performance testing
in the 7 MHz to 15 MHz frequency range**

Figure D.1 illustrates a phantom containing low-echo spheres, which meets the specifications in this Technical Specification. Figure D.2 shows an image made with the phantom, in which low-echo spheres are clearly visible as black spots without internal reflections.

**Key**

1	3,5 cm radius of curvature
2	0,5 cm radius of curvature
3	6-mm thick acrylic plate
4	flat scanning window
5	plate-glass reflector
6	alumina reflector
7	2-mm diameter anechoic spheres (8 per millilitre)

Figure D.1 – End- and top-view diagrams of the phantom containing 2 mm-diameter, low-echo spheres for use in the 7 MHz to 15 MHz frequency range

This prototype phantom was produced with one plate-glass reflector and one parallel, alumina (Al_2O_3)-plate reflector. The alumina reflector has a very high density and acoustic propagation speed, providing total internal reflection for angles of incidence as small as 16° , as compared to about 30° for glass.

In Figure D.2 the C8-5 transducer designation implies that the pulse spectrum lies in the 5 MHz to 8 MHz range. The vertical set of echoes occur at the surface of the alumina reflector.



Figure D.2 – Image obtained by using the phantom containing 2 mm-diameter, low-echo spheres and a pediatric transducer with a radius of curvature of about 1,5 cm

Annex E (informative)

Determination of low-echo sphere positions to within $D/8$ in x , y and z Cartesian coordinates

E.1 Procedure

With reference to 3.9, defining **depth interval**, Figure 1 and Figure B.2 d), the determination of low-echo sphere positions to within $D/8$ in x , y and z Cartesian coordinates can be accomplished via the following steps [7], repeating for all values of n .

NOTE The subscript index n is suppressed in Annex E.

- 1) For each digitized image and for each volume segment determined by the **depth interval**, d , compute the mean M_d and standard deviation SD_d of all $MPVs$ with centres lying within each volume segment, using the entire image set.
- 2) For each MPV_{ijk} , identify six nearest $MPVs$ and determine whether all seven $MPVs$, including itself, are at least 1,5 standard deviations below the mean established in step 1. Each such set of seven $MPVs$ is taken to be associated with a single low-echo sphere. See E.2.
- 3) Typically, a set of seven $MPVs$ determined in step 2 will have common positions with other such sets of seven $MPVs$ found in step 2. Associate all such sets with one low-echo sphere.
- 4) For sets of seven $MPVs$ corresponding to step 3, compute the best estimate for the position of the low-echo sphere centre by computing the Cartesian coordinates of the "centre of mass" (x_{CM} , y_{CM} and z_{CM}) as in Formulae (E.1), (E.2) and (E.3).

$$x_{CM,d} = \frac{\sum_{(ijk)_1}^{(ijk)_7} i \frac{D}{4} [M_d - (MPV)_{ijk}]}{\sum_{(ijk)_1}^{(ijk)_7} [M_d - (MPV)_{ijk}]} \quad (E.1)$$

$$y_{CM,d} = \frac{\sum_{(ijk)_1}^{(ijk)_7} j \frac{D}{4} [M_d - (MPV)_{ijk}]}{\sum_{(ijk)_1}^{(ijk)_7} [M_d - (MPV)_{ijk}]} \quad (E.2)$$

$$z_{CM,d} = \frac{\sum_{(ijk)_1}^{(ijk)_7} k \frac{D}{4} [M_d - (MPV)_{ijk}]}{\sum_{(ijk)_1}^{(ijk)_7} [M_d - (MPV)_{ijk}]} \quad (E.3)$$

where

- d is a running integer denoting the **depth interval** of interest, $d = 1, 2, 3 \dots$
- D is the diameter of the low-echo spherical inclusions, as defined in 3.4;

- M_d is the mean of all $MPVs$ with centres lying within a volume segment, determined by the **depth interval**, d , using the entire image set, as defined above;
- $(MPV)_{ijk}$ is the MPV at the ijk -site, as defined in 8.2.

E.2 Argument for the choice of seven MPV nearest-neighbour sites for determining the centres of low-echo spheres

Given that the sites involved should approximate a sphere with all sites lying inside a sphere of diameter D and all sites are at least 1,5 standard deviations (SD_d) below the mean (M_d) of all $MPVs$ with centres lying within the volume segment determined by the **depth interval** d (see steps 1 and 2 in Annex D), the possibilities are

- 1) a single site,
- 2) eight sites at the corners of a cube with side $D/4$,
- 3) seven sites defining the centre and corners of a tetrahedron (as employed),
- 4) nine sites, one at the centre and eight on the corners of a cube with side $D/2$.

A single site (option 1) is unacceptable because random fluctuations in the background speckle would trigger an overwhelming number of false positives.

Option 2 is a possible choice with the greatest distance between two sites (at opposite corners of the cube) being $(3/16)^{1/2} D = 0,43 D$.

For option 3 (the one used in the software), the maximum distance between sites is $D/2$, slightly greater than for option 2.

The maximum distance between sites for option 4 is $(3/4)^{1/2} D = 0,87 D$. This distance is considered to be too large when considering finite beam widths in the lateral and elevational dimensions and finite pulse length in the axial dimension – plus partial volume effects due to the spherical geometry of the low-echo inclusions and the statistical nature of the speckle pattern; thus, it is unlikely that the $MPVs$ at all 8 corner sites would be less than $M_d - 1,5 SD_d$ for less detectable low-echo spheres.

Using option 3, it was found that the number of low-echo spheres detected in any volume segment determined by the **depth interval** generally agrees with the mean number expected. Thus, almost all spheres detected by human observers in the image sets were detected by the software. Option 2 might be addressed in future work for comparison with option 3.

Annex F (informative)

Test of total internal reflection produced by alumina and plate-glass, plane reflectors

To test the effectiveness of the plate-glass and alumina reflectors at producing total internal reflection such that – for sufficiently small angles of incidence (90° being perpendicular incidence) – mode conversion to shear waves or Rayleigh waves does not occur, a phantom was constructed with parallel alumina and plate-glass reflectors at opposite ends. The phantom was filled with tissue-mimicking background material (no low-echo spheres). The surfaces of the vertical plates were about 23 cm apart, and two scanning windows existed on the top of the phantom. One scanning window had a 1 cm radius of curvature (ROC), half-cylindrical shape centred 5 cm from the plate-glass reflector and the other was flat and had dimensions 5 cm \times 10 cm with its centre line 5 cm from the alumina reflector. The curved window provided for coupling of a 1 cm ROC curved array with a sector angle of about 153° and the flat window allowed coupling of a phased array with a sector angle of about 90° . Thus, images could be created in which only one reflector was involved and the other side of the phantom consisted entirely of tissue-mimicking material.

NOTE 1 The alumina reflector in the phantom described had a surface roughness of 6 μm , according to the manufacturer.

Regarding the tissue-mimicking material in the phantom, the component materials were the same as in the phantoms containing low-echo spheres, except that the volume percentage of 3:1 ultra-filtered milk was reduced by a factor of 4/5 to yield an (attenuation coefficient)/frequency value of $\alpha f \approx 0,39 \text{ dB cm}^{-1} \text{ MHz}^{-1}$ instead of $0,5 \text{ dB cm}^{-1} \text{ MHz}^{-1}$, so that the penetration depth was greater, assuring availability of sufficient data for analyses. Measurements were carried out at 22°C and 5 MHz using a previously described procedure [10]. The propagation speed was $c = 1\,539 \text{ m s}^{-1}$, and $\alpha f = 0,39 \text{ dB cm}^{-1} \text{ MHz}^{-1}$.

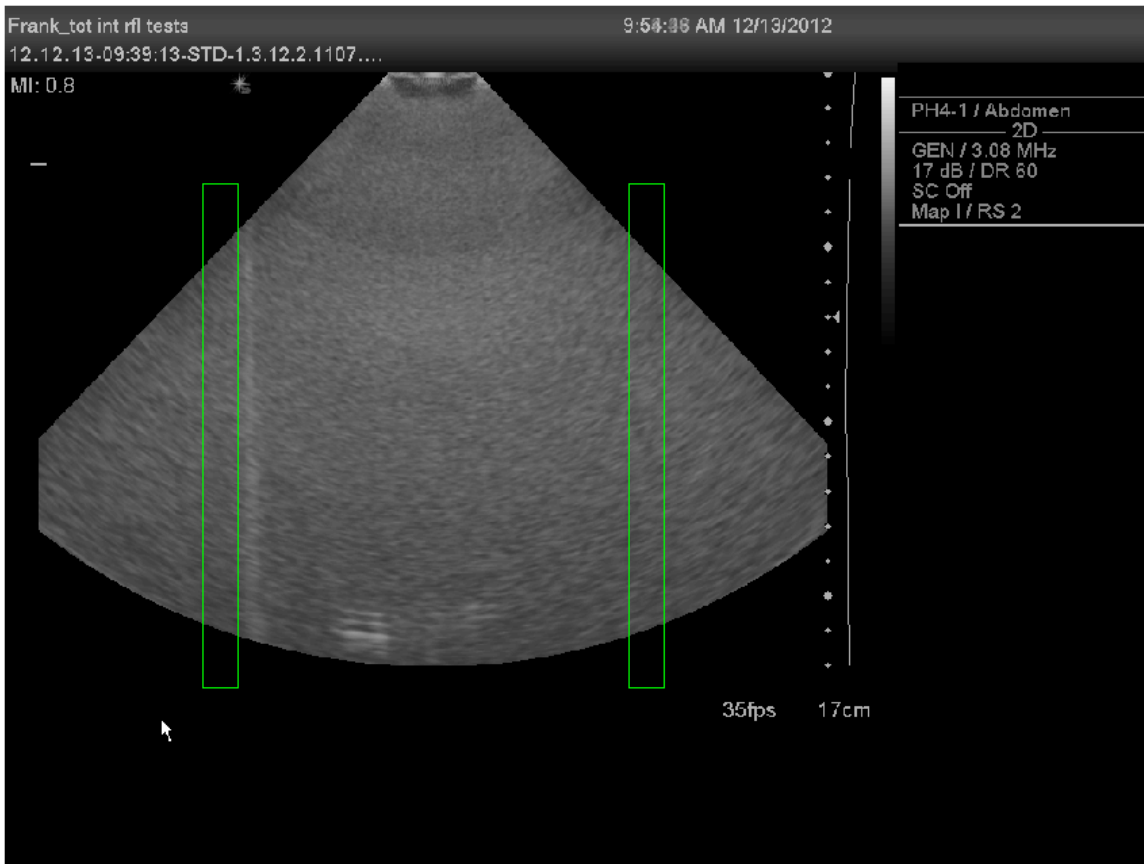
An average over 10 images obtained by using the phased array is shown in Figure F.1. Two rectangular areas 10 mm wide represent areas where mean pixel values over 5 mm vertical depth increments were computed.

NOTE 2 The mean pixel value in Annex F does not refer to *MPV* defined in 3.8.

The two rectangles have equal dimensions and are at the same positions vertically; however, one is just to the left of the vertical line of barely visible, diffuse reflections arising at the surface of the plate-glass reflector (left side in the image), and both rectangles are displaced by the same distance from the vertical axis of symmetry of the image. Thus, if total internal reflection were perfect – and the imaging were perfect, then graphs of the mean pixel values over 5 mm vertical depth increments versus vertical depth would be identical. Since there may be asymmetry of the phased array sensitivity, the two graphs may not be identical. Thus, the transducer was rotated 180° about a vertical axis and another set of 10 images was obtained and averaged. With rotation of the transducer, the plate-glass reflector appears on the right side of the image.

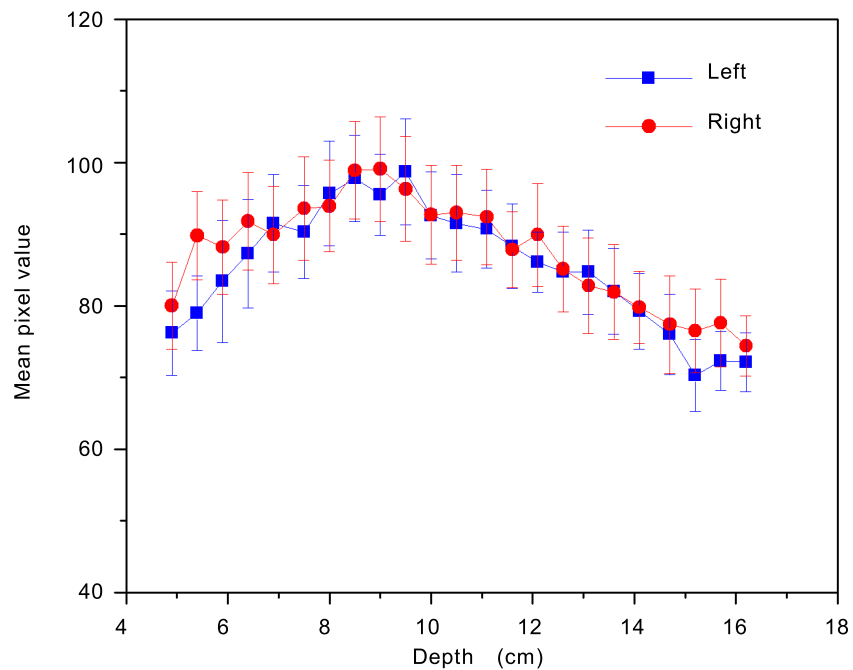
Figure F.2 shows graphs of the mean pixel values for the left and right rectangles. Note that the mean pixel values over 5 mm deep rectangles are zero except between about 5 cm and 16 cm (vertical distances). Figure F.3 shows the corresponding graphs after rotation of the transducer.

In Figure F.1 the plate-glass reflector is on the left (faint vertical line of diffuse reflections at the surface of the reflector). Green rectangles show where mean pixel values were computed over 5 mm vertical increments.



IEC

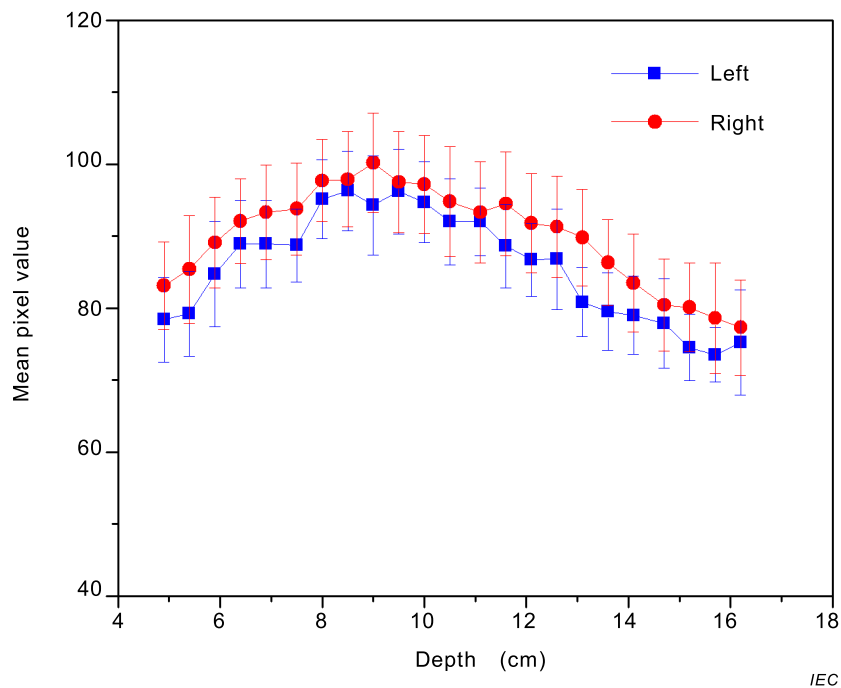
Figure F.1 – Average of 10 images obtained by using a phased array



IEC

The ordinate label is mean pixel value, and the abscissa label is vertical depth. Pixel-value standard-deviation bars for each 5 mm-depth interval are also shown.

Figure F.2 – Plot of the data with blue data computed in the left rectangle in Figure F.1 and red data computed in the right rectangle



The ordinate label is mean pixel value, and the abscissa label is vertical depth. Pixel-value standard-deviation bars for each 5 mm-depth interval are also shown.

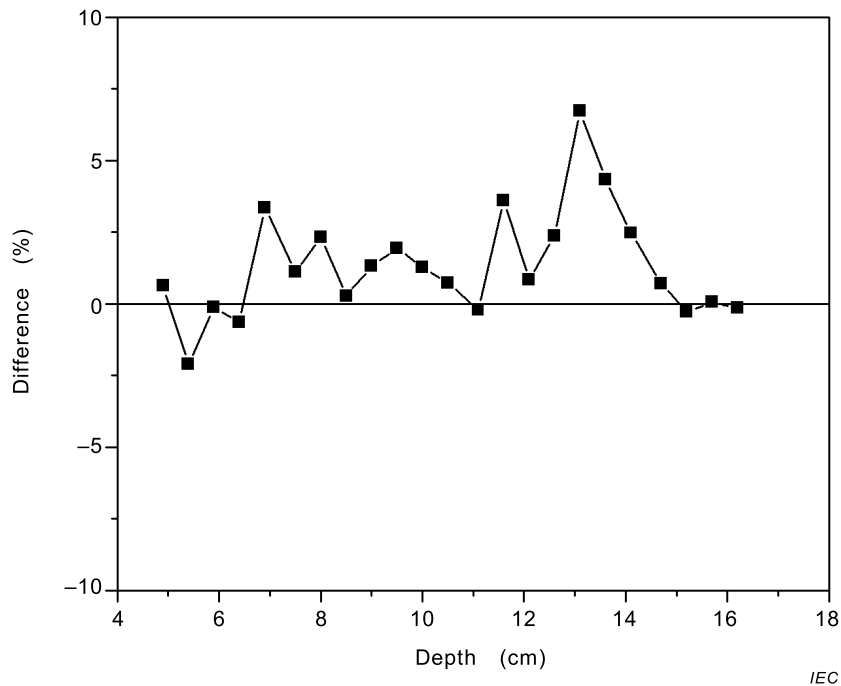
Figure F.3 – Plot of the data when the reflector is on the right side with blue computed in the left rectangle and red computed in the right rectangle

The percentage by which the mean pixel values resulting from reflections differ from the mean pixel values not involving reflections, where asymmetry of transducer sensitivity is corrected, can be derived from the data in Figures F.2 and F.3 using Formula (F.1). The results appear in Figure F.4.

$$\frac{1}{2} \sum_{i=1}^2 \frac{R_i - N_i}{N_i} \times 100\% \quad \frac{1}{2} \sum_{i=1}^2 \frac{R_i - N_i}{N_i} \times 100\% \quad (\text{F.1})$$

where

R_i and N_i are the mean pixel values on the reflector side and non-reflector side, respectively, and $i = 1$ corresponds to the reflector being on one side, and $i = 2$ corresponds to the reflector being on the other side.



Asymmetry of transducer sensitivity has been corrected using the data in Figures F.2 and F.3 and Formula (F.1). The ordinate label is difference (%), and the abscissa label is vertical depth (cm).

Figure F.4 – The percentage by which the mean pixel values resulting from reflections differ from the mean pixel values not involving reflections

What is addressed in Figure F.4 is the small contrast between the mean pixel value (corrected for transducer asymmetry) with the reflector involved ($CMPV_r$) and the mean pixel value (corrected for transducer asymmetry) without involvement of the reflector ($CMPV_o$). The relation between $CPMV$ and monitor luminance μ is not known to the authors. A conservative guess regarding the relation is that $(CPMV)^2$ is proportional to μ ; thus,

$$10 \log_{10} (\mu_r / \mu_o) = 20 \log_{10} (CMPV_r / CMPV_o),$$

where

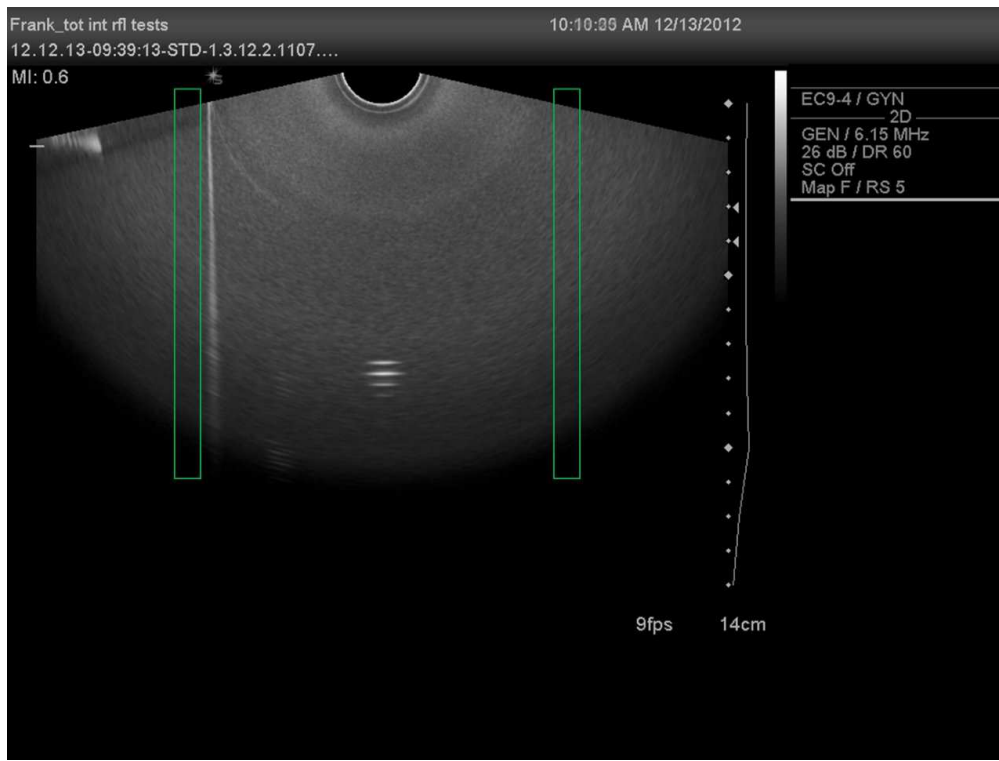
μ_r is the mean **pixel** luminance with involvement of the reflector, and

μ_o is the mean **pixel** luminance without involvement of the reflector.

From Table 1 in reference [11] image contrast equals object contrast at 1 dB and 2 dB, and obviously when the object contrast is 0 dB, image contrast and corrected mean pixel value contrast are 0 dB. (See pages 119 and 120 of reference [11] for definitions of object contrast and image contrast.). Again referring to Table 1 of reference [11], when the image contrast lies between 1 dB and -1 dB, the image contrast was not detectable by human observers.

From Figure F.4, $-0,22 \text{ dB} \leq 20 \log_{10} (CMPV_r / CMPV_o) \approx 10 \log_{10} (\mu_r / \mu_o) \leq 0,59 \text{ dB}$, and the contrasts are not detectable by human observers.

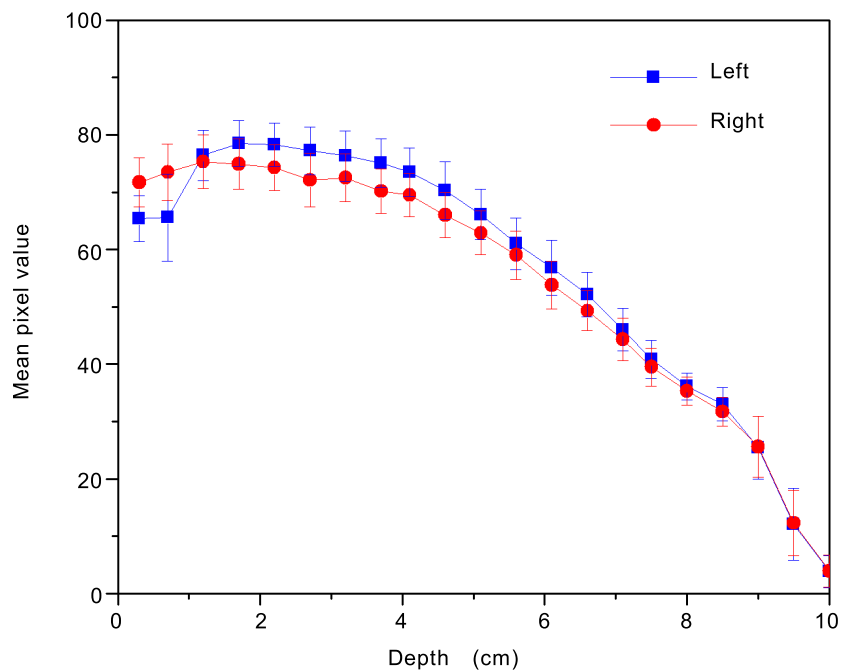
Figures. F.5, F.6 and F.7 correspond to Figures. F.1, F.2 and F.3, where the transducer is a curved array with a 1 cm-radius of curvature and the reflector is made of alumina. The sector angle is about 153°. Total internal reflection fails for sector angles greater than about 138°, corresponding to angles of incidence between 69° and 90°, as evidenced in the upper left side of the image in Figure F.5, distal to the reflector.



IEC

Total internal reflection fails for sector angles greater than about 138°, corresponding to angles of incidence between 69° and 90°, as evidenced in the upper left side of the image, distal to the reflector.

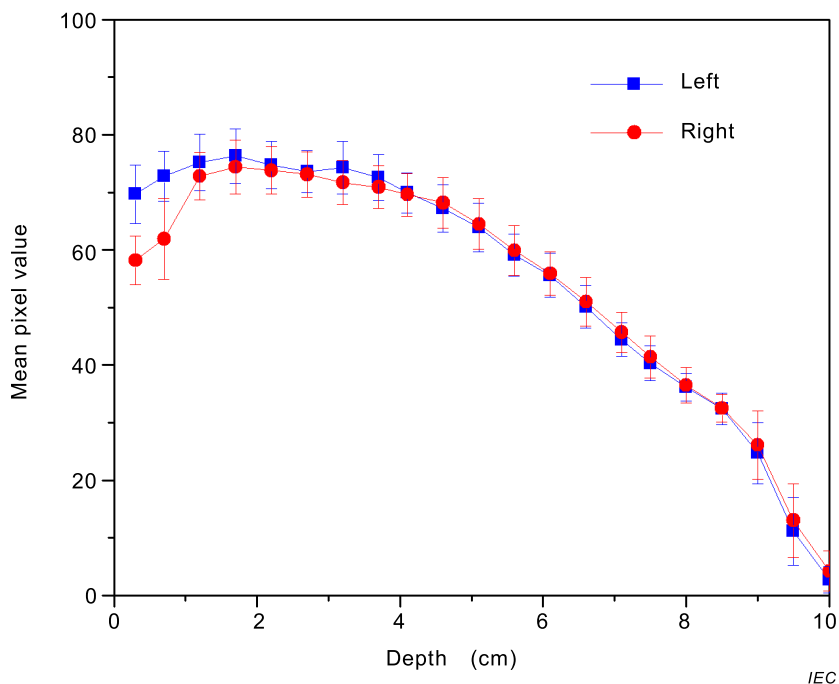
Figure F.5 – Wide sector (153°), 1 cm-radius-of-curvature transducer with alumina reflector on the left



IEC

The ordinate label is mean pixel value, and the abscissa label is vertical depth. Pixel-value standard-deviation bars for each 5 mm-depth interval are also shown. Note that for the vertical depth from 0 cm through 1 cm, total internal reflection fails.

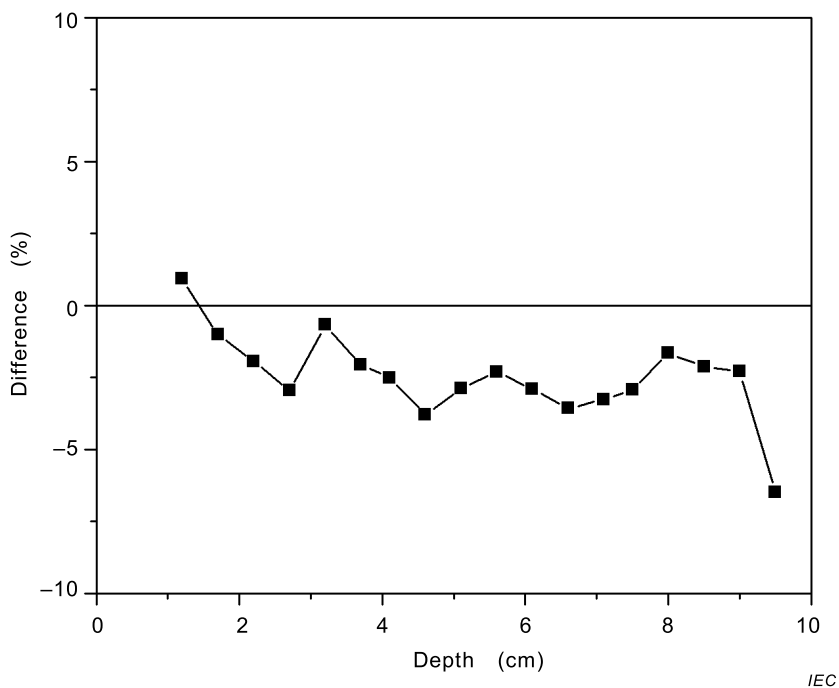
Figure F.6 – Plot of the data with blue computed in the left rectangle in Figure F.5 and red computed in the right rectangle



Again, for the depth from 0 cm through 1 cm, total internal reflection fails. The ordinate label is mean pixel value, and the abscissa label is vertical depth.

Figure F.7 – Plot of the data when the reflector is on the right side with blue computed in the left rectangle and red computed in the right rectangle

Figure F.8 shows the percentage by which the mean pixel values resulting from reflections differ from the mean pixel values not involving reflections, where asymmetry of transducer sensitivity has been corrected; corrections were derived from Figures F.6 and F.7 by using Formula (F.1).



Asymmetry of transducer sensitivity has been corrected using the data in Figures F.6 and F.7 and Formula (F.1). The ordinate label is difference (%), and the abscissa label is vertical depth (cm).

Figure F.8 – The percentage by which the mean pixel values resulting from reflections differ from the mean pixel values not involving reflections

Referring to the discussion involving Figure F.4 above, and employing the results shown in Figure F.8, we find $-0,63 \text{ dB} \leq 20 \log_{10} (CMPV_r / CMPV_o) \approx 10 \log_{10} (\mu_r / \mu_o) \leq 0,17 \text{ dB}$ and the contrasts are again not detectable by human observers.

Annex G (informative)

Results of a test of reproducibility of $LSNR_m$ versus depth for a phantom with 4 mm-diameter low-echo spheres and 2 spheres per millilitre

The following results are presented for comparison with those presented in Annex B, which were obtained with a phantom with 4 mm-diameter, low-echo spheres but only one such sphere per millilitre. Figure G.1 is an image using a curved array operating at 4,2 MHz with a phantom having two plate-glass reflectors. There are two low-echo spheres per millilitre instead of one such sphere per millilitre. Rather good reproducibility results are shown in Figure G.2.

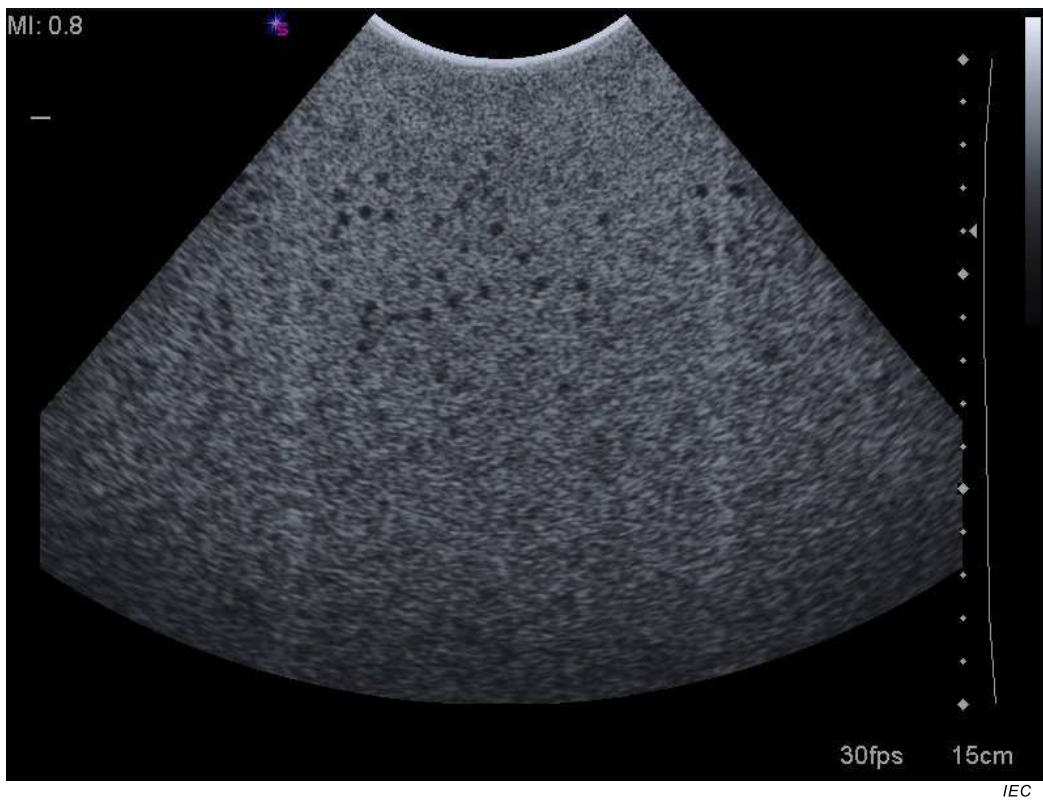
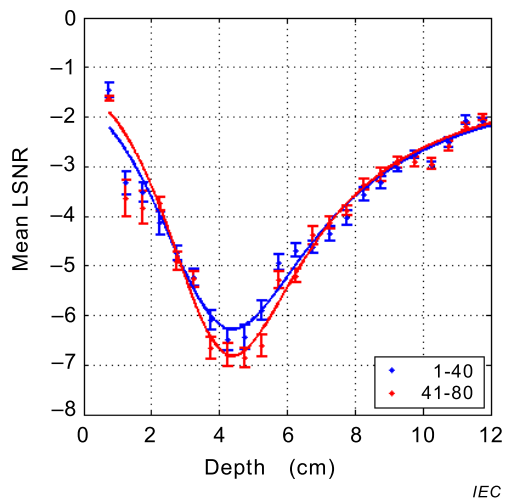
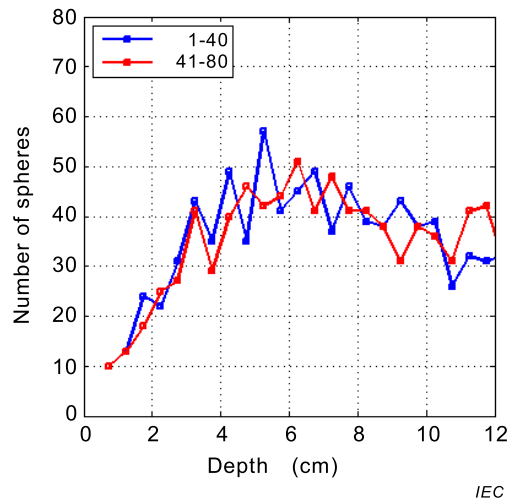


Figure G.1 – Example image of the phantom with a 4,2 MHz curved array
and two low-echo spheres per millilitre



a) Mean LSNR ($LSNR_m$)-values as a function of depth



b) Number of low-echo sphere centres detected in each 5 mm-depth interval

In the notation adopted in 8.3.2, read $LSNR_m$ for Mean LSNR at the ordinate label of the left graph.

Figure G.2 – Reproducibility results corresponding to the image set, one of which is shown in Figure G.1

Annex H (informative)

Results for low-echo sphere-concentration dependence of $LSNR_m$ versus depth for phantoms with 4 mm-diameter spheres

One phantom made in July 2011 has an average of one 4-mm diameter, **low-echo sphere** per millilitre and a second phantom made in October 2012 has an average of two such spheres per millilitre. Example images from the data sets are shown in Figures H.1 and H.3, and plots of $LSNR_m$ -values versus depth and number of detected **low-echo spheres** in each 5 mm-**depth interval** are shown in Figures H.2 and H.4. Image acquisition parameters were the same for 1 ml^{-1} and 2 ml^{-1} cases, and those parameters correspond to ordinary B-scans with no special processing such as spatial compounding or tissue harmonic imaging. The focus was at 4 cm.

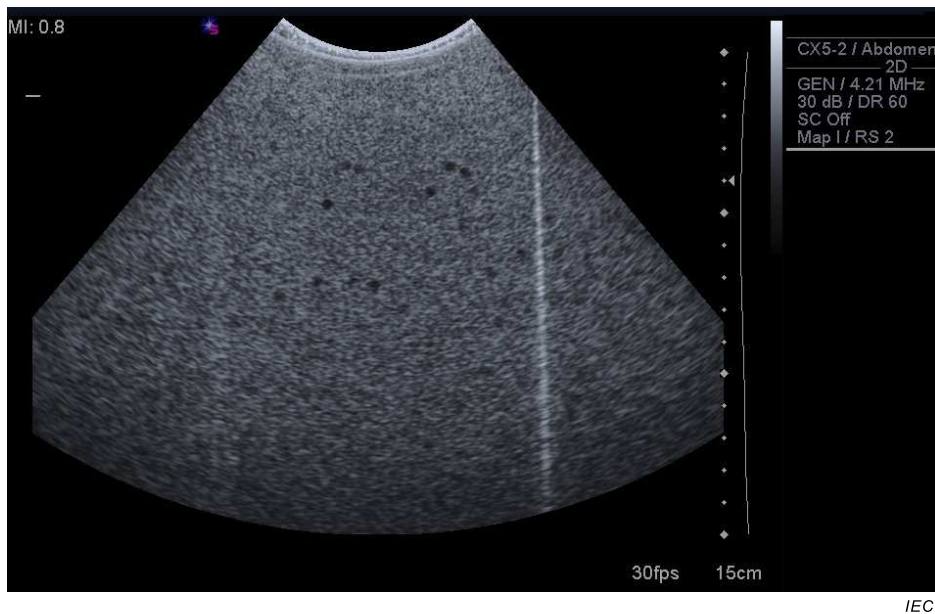
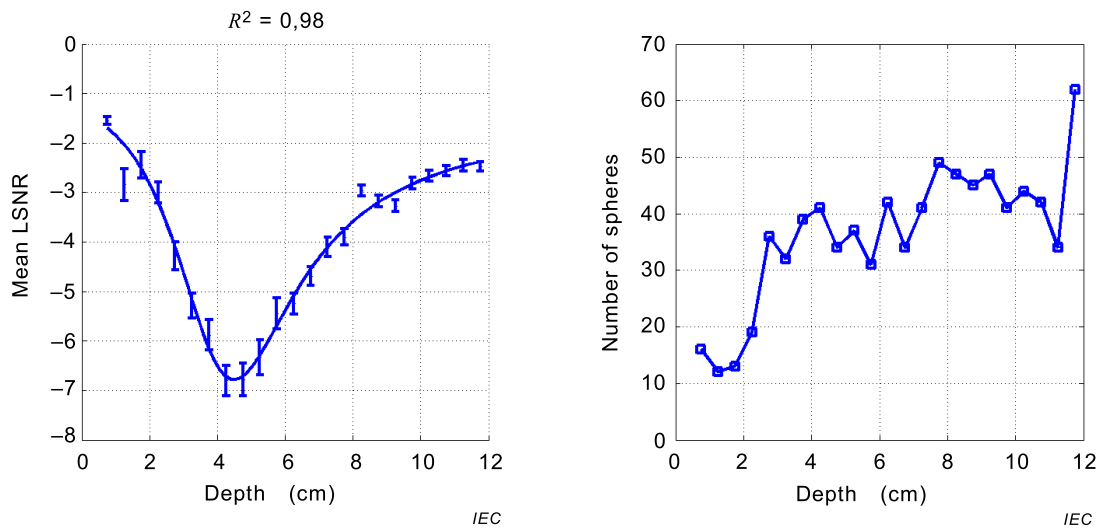


Figure H.1 – Example of an image from the image set giving rise to the results in Figure H.2; the phantom contained an average of one 4 mm-diameter, low-echo sphere per millilitre

In Figure H.2 R^2 is the coefficient of determination. $R^2 = 0$ if the data values and curve-fit values at the corresponding depths are completely uncorrelated, and $R^2 = 1$ if the two sets of values are completely correlated [12].



a) Mean LSNR ($LSNR_m$)-values versus depth for an average of one 4 mm-diameter, low-echo sphere per millilitre
 b) Number of low-echo sphere centres detected in each 5 mm-depth interval

In the notation adopted in 8.3.2, read $LSNR_m$ for Mean LSNR at the ordinate label of the left graph.

Figure H.2 – Results corresponding to an image set, one of which is shown in Figure H.1

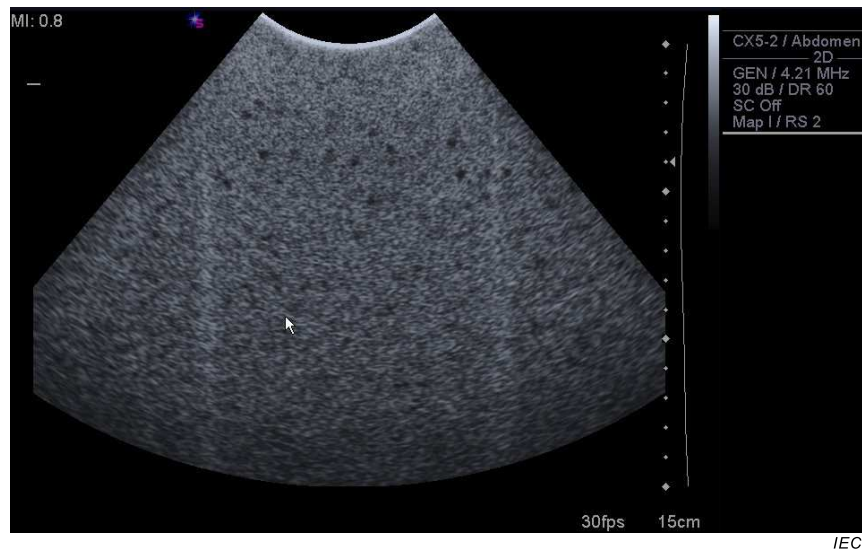
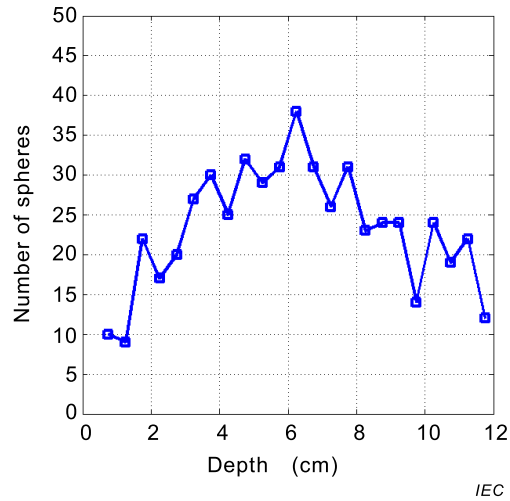
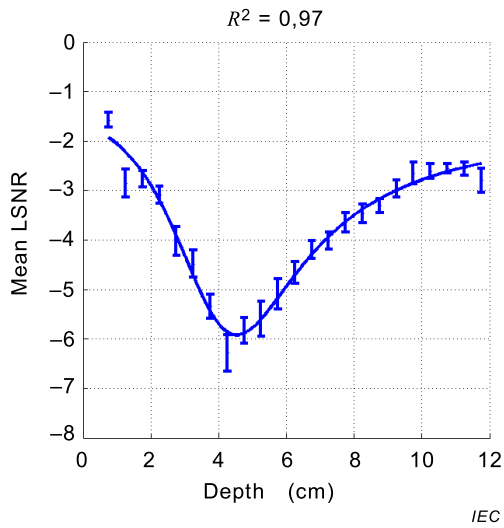


Figure H.3 – Example of an image from the data set giving rise to the results in Figure H.4; the phantom contained an average of two 4 mm-diameter, low-echo spheres per millilitre



a) Mean LSNR ($LSNR_m$)-values versus depth for an average of two 4 mm-diameter, low-echo spheres per millilitre

b) Number of low-echo sphere centres detected in each 5 mm-depth interval

In the notation adopted in 8.3.2, read $LSNR_m$ for Mean LSNR at the ordinate label of the left graph. R^2 is the coefficient of determination, defined in the text above Figure H.2.

Figure H.4 – Results corresponding to an image set, one of which is shown in Figure H.3

A concentration dependence is apparently demonstrated with the minimum $LSNR_m$ -value for the 1 ml^{-1} phantom at about $-6,7$ and for the 2 ml^{-1} phantom at about $-6,0$. The number of images employed for the 1 ml^{-1} case is twice that of the 2 ml^{-1} case, which means the expected number of low-echo spheres for each volume segment determined by the **depth interval** is the same for each. At 4 cm depth, based on the average number of spheres per millilitre, the volume addressed is about 45 ml for both 1 ml^{-1} and 2 ml^{-1} phantoms. Notice that the observed number at 4 cm depth for the 1 ml^{-1} case is about 35 and for the 2 ml^{-1} case is about 28. The difference could be attributed to pairs of spheres being close enough together that they are assumed to be one sphere and the "centre of mass" is somewhere between the two spheres' centres resulting in an $LSNR_n$ -value that is less negative than is appropriate. Investigation of this concentration dependence is ongoing and may result in alteration of the software to detect such pairings of spheres, so they can be eliminated from consideration.

See Annex I where a much better controlled experiment was done to assess concentration dependence using three phantoms containing 3,2 mm-diameter, low-echo spheres.

Annex I (informative)

Results for low-echo sphere-concentration dependence of $LSNR_m$ versus depth for phantoms with 3,2 mm-diameter spheres

A set of three phantoms was made with flat scanning windows and average low-echo sphere concentrations of 1 ml^{-1} , 2 ml^{-1} and 4 ml^{-1} . All spheres were made at the same time. Care also was taken to ensure that the background materials in all phantoms were identical. Thus, no material bias should exist between phantoms.

Data images for all three phantoms were obtained with identical equipment and scan parameters, including the TGC settings. Image acquisition parameters were the same for the 1 ml^{-1} , 2 ml^{-1} and 4 ml^{-1} cases and those parameters correspond to ordinary B-scans with no special processing, such as spatial compounding or tissue harmonic imaging. The focus was at 9 cm.

Results are shown in Figures I.1 to I.6. 280 images were used for the 1 ml^{-1} phantom, 140 images for the 2 ml^{-1} phantom and 75 images for the 4 ml^{-1} phantom. (Recall that the low-echo sphere density is 2 ml^{-1} for the phantom containing 3,2 mm-diameter spheres, for which results are shown in Figures C.1 to C.7.)

In terms of the most negative $LSNR_m$ curve-fitted values, the 4 ml^{-1} phantom has a minimum at $-11,3$, the 2 ml^{-1} phantom has a minimum at $-11,6$, and the 1 ml^{-1} phantom shows a minimum at $-12,6$. Thus, the most negative $LSNR_m$ -values span a range of only 11,5 % with a decrease in low-echo sphere concentration by a factor of 1/4, indicating that there is little dependence of even the most extreme $LSNR_m$ -values on such sphere concentration; therefore, it is reasonable to assume that the 2 ml^{-1} sphere concentration will yield acceptable accuracy. Note also that the correlation coefficient of $LSNR_m$ -values for 2 ml^{-1} (see Figure I.4) and corresponding $LSNR_m$ -values for 1 ml^{-1} (see Figure I.6) was computed, and is 0,985.

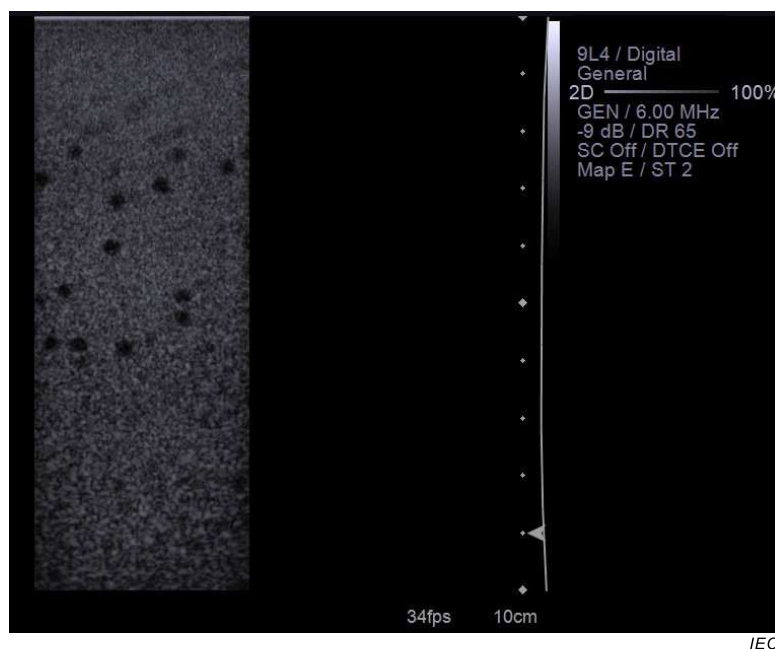
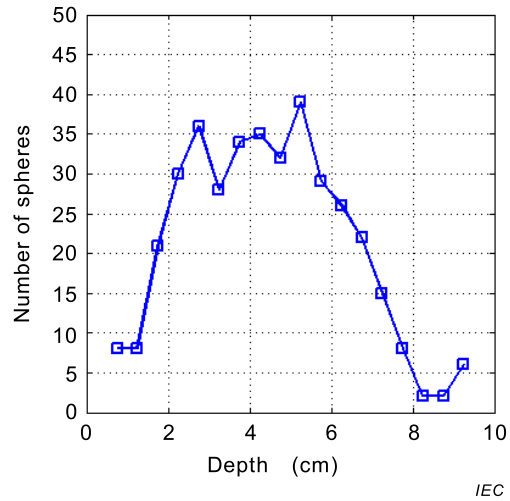
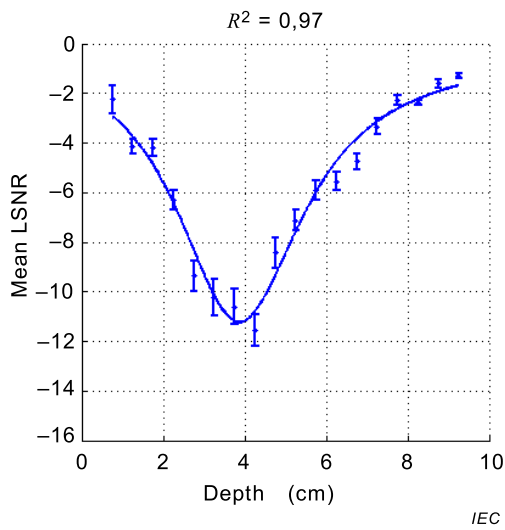


Figure I.1 – Example of an image from the 4 ml^{-1} data set producing the results shown in Figure I.2



a) Mean LSNR ($LSNR_m$)-values versus depth for an average of four 3,2 mm-diameter, low-echo spheres per millilitre

b) Number of low-echo sphere centres detected in each 5 mm-depth interval

In the notation adopted in 8.3.2, read $LSNR_m$ for Mean LSNR at the ordinate label of the left graph. R^2 is the coefficient of determination, defined in the text above Figure H.2.

Figure I.2 – Results for the phantom containing four 3,2 mm-diameter, low-echo spheres per millilitre

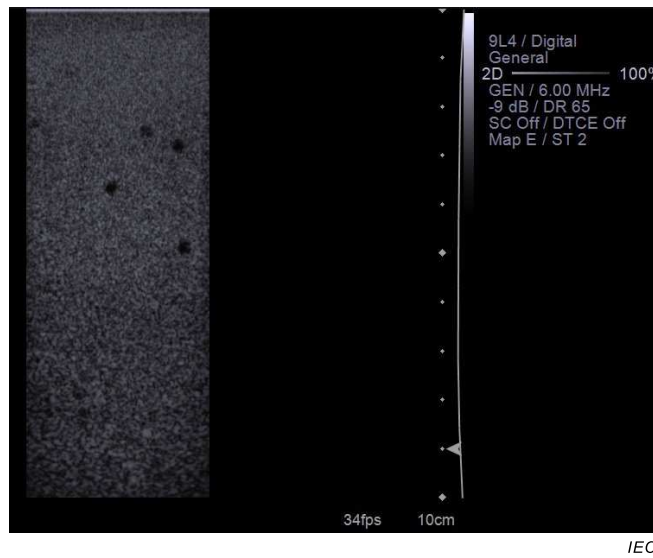
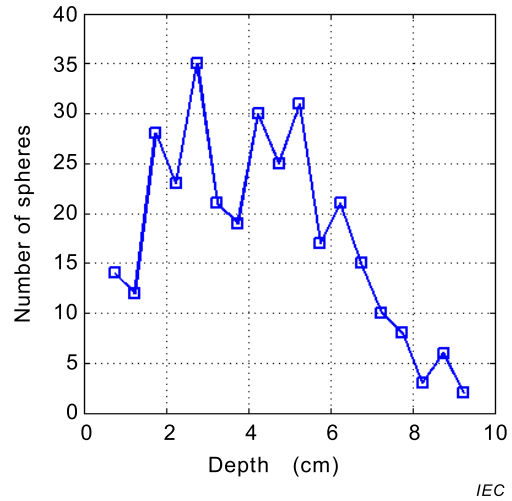
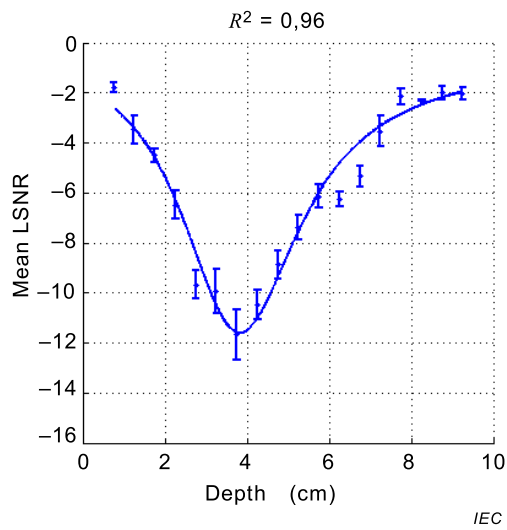


Figure I.3 – Example of an image from the 2 ml⁻¹ data set producing the results shown in Figure I.4



a) Mean LSNR ($LSNR_m$)-values versus depth for an average of two 3,2 mm-diameter, low-echo spheres per millilitre

b) Number of low-echo sphere centres detected in each 5 mm-depth interval

In the notation adopted in 8.3.2, read $LSNR_m$ for Mean LSNR at the ordinate label of the left graph. R^2 is the coefficient of determination, defined in the text above Figure H.2.

Figure I.4 – Results for the phantom containing two 3,2 mm-diameter, low-echo spheres per millilitre

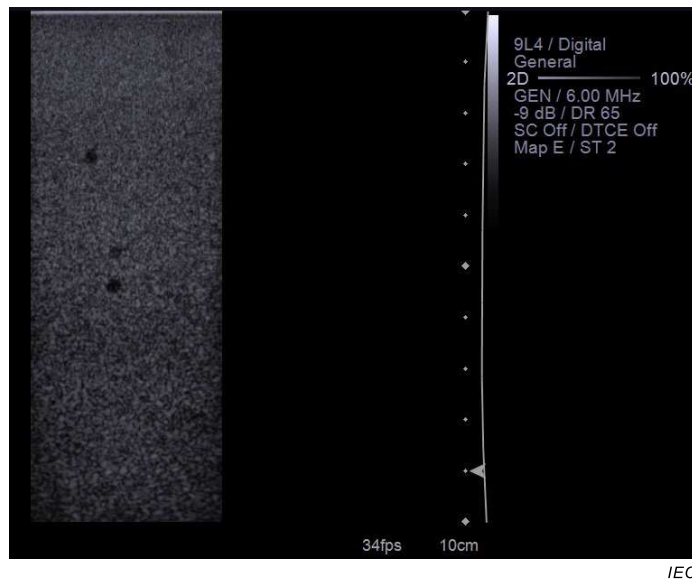
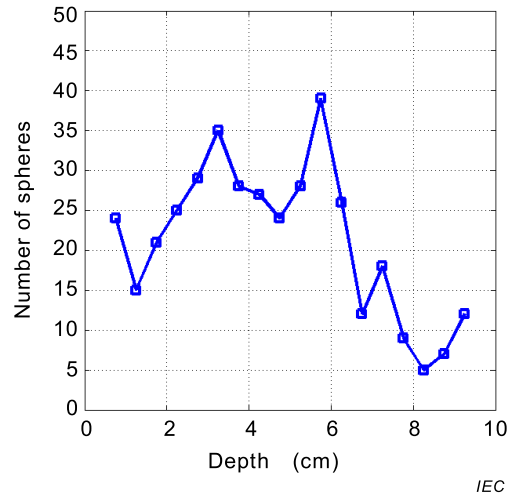
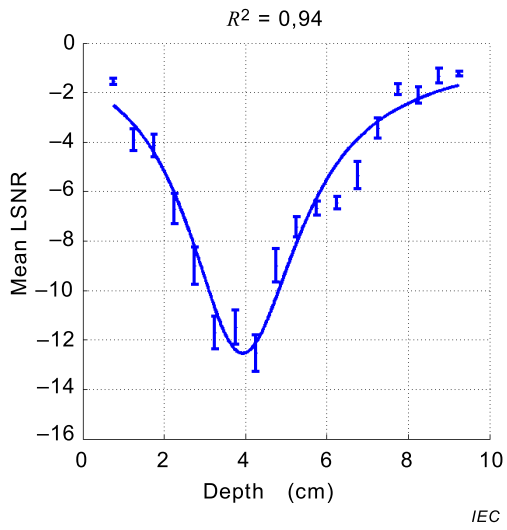


Figure I.5 – Example of an image from the 1 ml⁻¹ data set producing the results shown in Figure I.6



a) Mean LSNR ($LSNR_m$)-values versus depth for an average of one 3,2 mm-diameter, low-echo sphere per millilitre

b) Number of low-echo sphere centres detected in each 5 mm-depth interval

In the notation adopted in 8.3.2, read $LSNR_m$ for Mean LSNR at the ordinate label of the left graph. R^2 is the coefficient of determination, defined in the text above Figure H.2.

Figure I.6 – Results for the phantom containing one 3,2 mm-diameter, low-echo sphere per millilitre

Annex J (informative)

Comparison of two different makes of scanner with similar transducers and console settings

Standard B-mode images obtained with two different commercial ultrasound medical diagnostic systems were assessed for a focus at 4 cm and convex arrays with nearly the same sector angle. Also, the console settings were the same except for a small difference in nominal frequency. Figure J.1 illustrates results for the System A scanner and 7CF2 3-D transducer operated at 4,5 MHz in 2-D mode, and Figure J.2 illustrates results for the System B scanner with a 4DC7-3 3-D transducer operated at 4 MHz in 2-D mode. System A appears to outperform System B to a considerable extent.

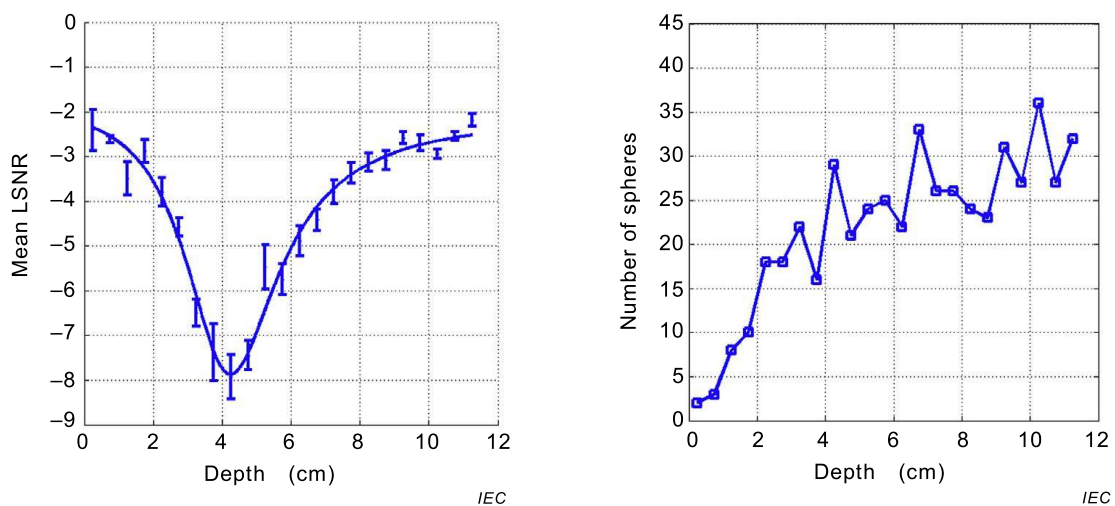


Figure J.1 – Results for System A scanner and 7CF2 3-D (swept convex array) transducer focused at 4 cm and operated at 4,5 MHz in 2-D mode

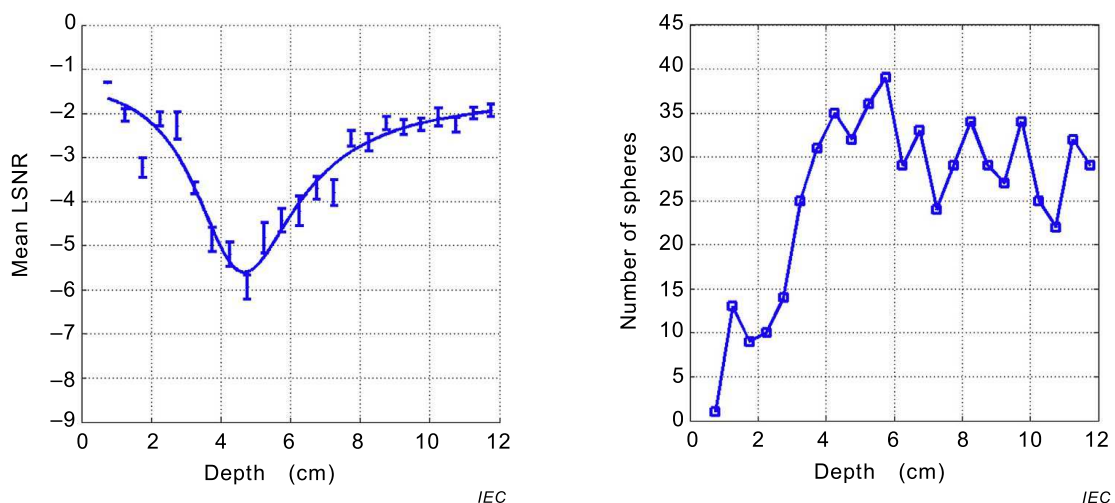


Figure J.2 – Results for System B scanner with a 4DC7-3 3-D (convex array) transducer, operated at 4 MHz in 2-D mode and focused at 4 cm. The sector angle and all other console settings mimicked those for the System A case (Figure J.1)

Keeping in mind that the more negative a Mean LSNR ($LSNR_m$) value is, the better the detectability of the low-echo sphere, ultrasound System A outperforms System B at all depths.

Also, the backscatter coefficient of the material composing the low-echo spheres is about –30 dB relative to that of the material composing the background.

All $LSNR_m$ values would be increased (made less negative) if the backscatter coefficient of the material composing the low-echo-spheres were increased. Consider an $LSNR_m$ value of –2 to be a threshold for human observer detection of the low-echo spheres. Then the increase in low-echo sphere backscatter coefficient needed to cause an increase of $-2 - (-7,8) = 5,8$ for System A at a 4 cm depth would be greater than the increase in low-echo sphere backscatter coefficient needed to cause an increase of $-2 - (-5) = 3$ for System B at a 4 cm depth. The implication is that System A would allow detectability for low-echo spheres having a higher backscatter coefficient than would System B.

Consider, for example, a tumour with dimensions greater than the low-echo sphere diameter D . For a range of values of (tumour backscatter coefficient)/(background backscatter coefficient), the tumour would be detectable by a human observer using System A, but not detectable using System B. Also, when the tumour is detectable, its boundary would be delineated with a resolution of D .

Annex K (informative)

Special considerations for 3-D probes

K.1 3-D probes operating in 2-D imaging mode

For 3-D mechanically driven probes, the scan plane should be at a known position and orientation relative to the housing of the linear array or convex array so that the scan plane can be made perpendicular to the direction of translation (in $D/4$ increments) of the transducer or phantom.

For 2-D arrays [2] the scan plane should be at a known position and orientation relative to the transducer and be such that the scan plane can be perpendicular to the direction of translation (in $D/4$ increments) of the transducer or phantom while the transducer surface remains entirely acoustically coupled to the phantom scanning window.

K.2 2-D arrays operating in 3-D imaging mode for determining $LSNR_m$ -values as a function of depth for reconstructed images

The entire emitting surface of the probe should be acoustically coupled to the scanning window at all times during $D/4$ translations of the probe or phantom, and a complete 3-D data set should be recorded at each position. Sets of reconstructed images with "scan planes" perpendicular to the translation direction, all of which are at the same position relative to the transducer, can then be analysed to yield $LSNR_m$ -values as a function of depth.

NOTE The large amount of data that needs to be stored may make this procedure impractical.

K.3 Mechanically driven 3-D probes operating in 3-D imaging mode

It is unlikely that $LSNR_m$ -values versus depth can be generated because it is unlikely that the entire emitting surface of the probe can be acoustically coupled to the scanning window at all times during $D/4$ translations of the probe or phantom.

Bibliography

- [1] Szabo TL. *Diagnostic Ultrasound Imaging: Inside Out – Second Edition*, Elsevier Academic Press, Burlington, Massachusetts, USA, 2014
 - [2] Madsen EL, Zagzebski JA, Macdonald MC, Frank GR, Ultrasound focal lesion detectability phantoms, *Med Phys*, vol. 18, pp. 1171–1180 (1991)
 - [3] Kofler JM Jr, Lindstrom MJ, Kelcz F, Madsen EL, Association of automated and human observer lesion detectability using phantoms, *Ultrasound Med Biol*, vol.31, p.351–359 (2005)
 - [4] Madsen EL, Insana MF, Zagzebski JA, Method of data reduction for accurate determination of acoustic backscatter measurements, *J Acoust Soc Am*, vol.76, p.913–923 (1984)
 - [5] Sigelmann RA, Reid JM, Analysis and measurement of ultrasound backscattering from an ensemble of scatterers excited by sine-wave bursts, *J Acoust Soc Am*, vol.53, p.1351–1355 (1973)
 - [6] Morse PM, Feshbach H, *Methods of theoretical physics*, McGraw-Hill, New York, 1953, (see Chapter 9, p.1066)
 - [7] Madsen EL, Song C and Frank GR, Low-echo sphere phantoms and methods for assessing imaging performance of medical ultrasound scanners, *Ultrasound Med Biol*, vol.40, p.1697–1717 (2014)
 - [8] Pianykh OS, *Digital imaging and communications in medicine (DICOM): A practical introduction and survival guide*, Springer, Berlin, 2012
 - [9] Kofler JM Jr, Madsen EL, Improved method for determining resolution zones in ultrasound phantoms with spherical simulated lesions, *Ultrasound Med Biol*, vol.27, p.1667–1676 (2001)
 - [10] Madsen EL, Dong F, et al., Interlaboratory comparison of ultrasonic backscatter, attenuation, and speed measurements, *J Ultrasound Med* vol.18, p.615–631, 1999 (see pages 617 and 618 UWLMP section)
 - [11] Hall TJ, Insana MF, Soller mm, and Harrison LA, "Ultrasound contrast detail analysis: A preliminary study in human observer performance," *Med Phys* vol. 20, pp 117–127 (1993)
 - [12] Dawson B and Trapp RG, *Basic & Clinical Biostatistics*, 4th edition, McGraw-Hill, New York, 2004
-

INTERNATIONAL
ELECTROTECHNICAL
COMMISSION

3, rue de Varembé
PO Box 131
CH-1211 Geneva 20
Switzerland

Tel: + 41 22 919 02 11
Fax: + 41 22 919 03 00
info@iec.ch
www.iec.ch